

1 **Global assessment of climatic responses to the ozone-vegetation**  
2 **interactions**

3

4 Xinyi Zhou<sup>1</sup>, Xu Yue<sup>1</sup>, Chenguang Tian<sup>1</sup>, Xiaofei Lu<sup>1</sup>

5

6 <sup>1</sup> Jiangsu Key Laboratory of Atmospheric Environment Monitoring and Pollution  
7 Control, Collaborative Innovation Center of Atmospheric Environment and Equipment  
8 Technology, School of Environmental Science and Engineering, Nanjing University of  
9 Information Science & Technology, Nanjing, 210044, China

10

11 *Corresponding author: Xu Yue (Email: [yuxu@nuist.edu.cn](mailto:yuxu@nuist.edu.cn))*

12 **Abstract.** The coupling between surface ozone (O<sub>3</sub>) and vegetation significantly  
13 influences regional to global climate. O<sub>3</sub> uptake by plant stomata inhibits  
14 photosynthetic rate and stomatal conductance, impacting evapotranspiration through  
15 land surface ecosystems. Using ~~the~~ a climate-vegetation-chemistry coupled [model \(the](#)  
16 [NASA GISS ModelE2 coupled with Yale Interactive terrestrial Biosphere, or ModelE2-](#)  
17 [YIBs-model;\)](#), we assess the global climatic responses to O<sub>3</sub>-vegetation interactions  
18 during boreal summer of ~~2010s~~ [the present day](#) (2005-2014). High O<sub>3</sub> pollution reduces  
19 stomatal conductance, resulting in ~~the~~ warmer and drier conditions worldwide. The  
20 most significant responses are found in the eastern U.S. and eastern China, where ~~local~~  
21 ~~latent heat flux decreases by 8.17% and 9.48%, respectively. Consequently,~~ surface  
22 air temperature ~~rises~~ [increases](#) by  $+0.33 \pm 0.87$  °C and  $+0.56 \pm 0.38$  °C, ~~and~~ [respectively](#).  
23 [These temperature rises are accompanied by decreased latent heat and increased](#)  
24 sensible heat ~~flux rises by +16.54% and +25.46% in the two hotspot~~ [both](#) regions. The  
25 O<sub>3</sub>-vegetation interaction also affects atmospheric pollutants. Surface [maximum daily](#)  
26 [8-hour average](#) O<sub>3</sub> concentrations increase by  $+1.2646 \pm 3.02$  ppbv in eastern China and  
27 ~~+0.98~~ [1.15 ± 1.77](#) ppbv in eastern U.S. due to the O<sub>3</sub>-induced inhibition of stomatal  
28 uptake. With reduced atmospheric stability following the warmer climate, increased  
29 cloudiness but decreased relative humidity jointly reduce aerosol optical depth  
30 ~~(AOD)~~ [by -0.06 ± 0.01 \(-14.67 ± 12.15%\)](#) over eastern China. This study suggests that  
31 vegetation feedback should be considered for a more accurate assessment of climatic  
32 perturbations caused by tropospheric O<sub>3</sub>.

## 1 Introduction

Tropospheric ozone (O<sub>3</sub>), one of the most detrimental air pollutants (Myhre et al., 2013), not only poses threats to human health (Norval et al., 2011; Nuvolone et al., 2018) but also induces phytotoxic effects to vegetation (Mills et al., 2007; Pleijel et al., 2007). When exposed to certain levels of O<sub>3</sub>, plant photosynthesis and stomatal conductance is inhibited due to the O<sub>3</sub> oxidation of cellular, enzyme, and chlorophyll (Dizengremel, 2001; Fiscus et al., 2005; Jolivet et al., 2016). Consequently, the carbon assimilation of terrestrial ecosystems is limited (Yue and Unger, 2014; Oliver et al., 2018) and the land-air exchange rates of water and heat fluxes are altered (Lombardozzi et al., 2015).

Experimental studies have shown that the excessive O<sub>3</sub> exposure reduced both plant photosynthesis and stomatal conductance (Ainsworth et al., 2012; Lombardozzi et al., 2013). The reduction rates are dependent on the O<sub>3</sub> stomatal fluxes as well as the damaging sensitivities that vary among different vegetation types (Nussbaum and Fuhrer, 2000; Karlsson et al., 2004; Pleijel et al., 2004). ~~Traditional~~ Several exposure-based indexes ~~like~~ such as accumulated hourly O<sub>3</sub> concentrations over a threshold of 40 ppb (AOT40) ~~are widely~~ and sum of all hourly average concentrations (SUM00) are used to assess O<sub>3</sub>-induced vegetation damage (Fuhrer et al., 1997). ~~However, such~~ statistical schemes fail; Paoletti et al., 2007). In addition, the flux-related POD<sub>y</sub> method (phytotoxic O<sub>3</sub> dose above a threshold flux of y) is also widely applied to ~~account~~ for consider the dynamic adjustment of ~~vegetation physiological processes~~ stomatal conductance (Buker et al., 2015; Sicard et al., 2016). Taking into account the variability of plant sensitivities, different O<sub>3</sub> damage schemes were proposed to quantify the O<sub>3</sub> impacts on land carbon assimilation from regional to global scales (Anav et al., 2011; Lam et al., 2023; Lei et al., 2020). For example, Sitch et al. (2007) calculated the simultaneous damages to both photosynthesis and stomatal conductance based on the instantaneous O<sub>3</sub> stomatal uptake. In contrast, Lombardozzi et al. (2012) estimated the ~~inconsistent~~ decoupled reductions in plant photosynthesis and stomatal conductance using different response relationships to the cumulative O<sub>3</sub> stomatal uptake. Applications of different schemes resulted in a wide range of reductions in gross primary productivity (GPP) by 2-12% globally with regional hotspots up to 20-30%

63 (Lombardozzi et al., 2015; Unger et al., 2020; Zhou et al., 2024).

64 The O<sub>3</sub>-induced inhibition in stomatal conductance decreases dry deposition and  
65 consequently enhances surface O<sub>3</sub> concentrations (Clifton et al., 2020; Wesely and  
66 Hicks, 2000; Zhang et al., 2006). Using the Sitch et al. (2007) scheme with high O<sub>3</sub>  
67 damaging sensitivities in the ~~climate model ModelE2-YIBs~~, ModelE2-YIBs (NASA  
68 GISS ModelE2 coupled with Yale Interactive terrestrial Biosphere model), Gong et al.  
69 (2020) revealed that O<sub>3</sub>-vegetation interactions increased regional O<sub>3</sub> concentrations by  
70 1.8 ppbv in the eastern U.S., 1.3 ppbv in Europe, and 2.1 ppbv in eastern China for the  
71 year 2010. As a comparison, Sadiq et al. (2017) found ~~a consistent but~~ consistently  
72 ~~stronger positive~~ feedback on O<sub>3</sub> concentrations in these polluted regions using the  
73 scheme of Lombardozzi et al (2012) embedded in ~~a different climate model.~~  
74 ~~Inclusion~~ the Community Earth System Model (CESM). Moreover, the inclusion of  
75 online O<sub>3</sub>-vegetation interactions in numerical models will ~~cause stronger damages~~  
76 ~~to also result in a greater loss of simulated~~ land carbon assimilation due to the feedbacks  
77 of both ~~ecosystem~~ ecosystems and surface O<sub>3</sub>. This is attributable to several factors. On  
78 one hand, ~~the~~ O<sub>3</sub> damages to leaf photosynthesis inhibit plant growth and decrease leaf  
79 area index (LAI), leading to higher reduction percentage in GPP compared to  
80 simulations without LAI changes (Yue et al., 2020). On the other hand, the O<sub>3</sub>  
81 enhancement due to vegetation feedback may cause additional vegetation damage and  
82 result in further GPP losses (Lei et al., 2021). As a result, the O<sub>3</sub>-vegetation interactions  
83 should be considered in the global estimate of O<sub>3</sub> damages to ecosystem functions.

84 In addition to affecting surface O<sub>3</sub>, the O<sub>3</sub>-vegetation interaction can also alter the  
85 water and energy exchange between land and atmosphere. through the modulation of  
86 stomatal conductance. For example, Lombardozzi et al. (2015) used the Community  
87 Land Model (CLM) and estimated that the cumulative uptake of O<sub>3</sub> by the leaves  
88 resulted in reduction of 2.2% in transpiration but increase of 5.4% in runoff globally.  
89 Arnold et al. (2018) used ~~the Community Earth System Model (CESM)~~ CESM and  
90 found that plant exposure to O<sub>3</sub> could decrease the land-air moisture fluxes and  
91 atmospheric humidity, which further reduced shortwave cloud forcing in polluted  
92 regions and induced widespread surface warming up to +1.5 K. Two recent studies

93 utilized the WRF-chem model and revealed considerable warming and the associated  
94 meteorological perturbations due to the O<sub>3</sub>-vegetation interactions in China (Zhu et al.,  
95 2022; Jin et al., 2023). However, all these modeling studies applied the same O<sub>3</sub>  
96 vegetation damage scheme proposed by Lombardozzi et al. (2012). It's necessary to  
97 assess the climatic responses to O<sub>3</sub>-vegetation interactions using different schemes so  
98 as to explore the robust responses and the associated uncertainties.

99 In this study, we quantified the global impacts of O<sub>3</sub>-vegetation interaction on  
100 climatic conditions and surface air pollutants during 2010s using the ~~Earth-system~~  
101 ~~model-NASA-GISS-ModelE2-coupled-with-Yale-Interactive-terrestrial-Biosphere~~  
102 ~~(ModelE2-YIBs)-model~~ (Yue and Unger, 2015). This fully coupled framework was  
103 implemented with the semi-mechanistic O<sub>3</sub> damage scheme proposed by Sitch et al.  
104 (2007), which calculated ~~aggregate~~aggregated O<sub>3</sub> damage to photosynthesis based on  
105 varied sensitivities to ~~instant~~instantaneous stomatal O<sub>3</sub> uptake ~~for~~across eight plant  
106 functional types (PFTs). We performed sensitivity experiments to quantify the  
107 responses of surface air temperature and precipitation to O<sub>3</sub>-vegetation interaction. The  
108 feedbacks to aerosols and O<sub>3</sub> concentrations were also examined.

## 110 **2 Method**

### 111 **2.1 Model descriptions**

112 The ModelE2-YIBs is a fully coupled climate-carbon-chemistry model combining  
113 the NASA GISS ModelE2 with the YIBs vegetation model. ModelE2 is a general  
114 circulation model with the horizontal resolution of 2°×2.5° in latitude and longitude  
115 and 40 vertical layers up to 0.1 hPa. It dynamically simulates gas-phase chemistry (NO<sub>x</sub>  
116 - HO<sub>x</sub> - O<sub>x</sub> - CO - CH<sub>4</sub> - NMVOCs), aerosols (sulfate, nitrate, black and organic carbon,  
117 dust, and sea salt), and their interactions (Menon and Rotstayn, 2006). Both the physical  
118 and chemical processes are calculated every 0.5 h and the radiation module is called  
119 every 2.5 h. The radiation module includes direct and indirect aerosol radiative effects  
120 and accounts for absorption of multiple greenhouse gases (GHGs). For cloud optical  
121 parameters, it uses Mie scattering, ray tracing, and matrix theory (Schmidt et al., 2006).  
122 The model outperforms 20 other IPCC-class climate models in simulating surface solar

radiation (Wild et al., 2013) and has been extensively validated for meteorological and hydrological variables against observations and reanalysis data (Schmidt et al., 2014).

The YIBs model employs the well-established Farquhar model for leaf photosynthesis and Ball-Berry model for stomatal conductance (Farquhar et al., 1980; Ball et al., 1987) as follows:

$$A_{tot} = \min(J_c, J_e, J_s) \quad (1)$$

Here, the total leaf photosynthesis, denoted as  $A_{tot}$  ( $\mu\text{mol m}^{-2}$  [leaf]  $\text{s}^{-1}$ ), is calculated considering both  $C_3$  (Collatz et al., 1991) and  $C_4$  plants (Collatz et al., 1992). The  $A_{tot}$  is derived from the minimum value of the constraints. The ribulose-1,5-bisphosphate carboxylase (Rubisco) limited rate of carboxylation is  $J_c$ :

$$g_s = m \frac{(A_{tot} - R_d) \times RH}{e_s} + b J_c = \begin{cases} V_{cmax} \left( \frac{c_i - \Gamma_*}{c_i + K_c(1 + O_i/K_o)} \right) & \text{for } C_3 \text{ plant} \\ V_{cmax} & \text{for } C_4 \text{ plant} \end{cases} \quad (2)$$

The Here, the total leaf photosynthesis, denoted as  $A_{tot}$ , is calculated as the minimum value among the ribulose-1,5-bisphosphate carboxylase limited rate of carboxylation ( $J_c$ ), rate restricted by the availability of light limited rate ( $J_e$ ), and is  $J_e$ :

$$J_e = \begin{cases} a_{leaf} \times PAR \times \alpha \times \left( \frac{c_i - \Gamma_*}{c_i + 2\Gamma_*} \right) & \text{for } C_3 \text{ plant} \\ a_{leaf} \times PAR \times \alpha & \text{for } C_4 \text{ plant} \end{cases} \quad (3)$$

The export-limited rate ( $J_s$ ) for  $C_3$  plants and the phosphoenolpyruvate carboxylase (PEPC) limited rate of carboxylation for  $C_4$  plants are represented by  $J_s$ :

$$J_s = \begin{cases} 0.5 V_{cmax} & \text{for } C_3 \text{ plant} \\ K_s \times V_{cmax} \times \frac{c_i}{P_{atm}} & \text{for } C_4 \text{ plant} \end{cases} \quad (4)$$

In these functions,  $V_{cmax}$  ( $\mu\text{mol m}^{-2} \text{s}^{-1}$ ) is the maximum carboxylation capacity.  $c_i$  and  $O_i$  (Pa) represent the internal leaf  $\text{CO}_2$  and oxygen partial pressure.  $\Gamma_*$  (Pa) denotes the  $\text{CO}_2$  compensation point, while  $K_c$  and  $K_o$  (Pa) are Michaelis-Menten constants for the carboxylation and oxygenation of Rubisco, respectively. The parameters  $\Gamma_*$ ,  $K_c$ , and  $K_o$  vary with temperature based on the sensitivity of the vegetation to temperature ( $Q_{10}$  coefficient).  $PAR$  ( $\mu\text{mol m}^{-2} \text{s}^{-1}$ ) is the absorbed

143 photosynthetically active radiation,  $a_{leaf}$  is leaf-specific light absorbance that  
 144 considers sunlit and shaded leaves, and  $\alpha$  is quantum efficiency.  $P_{atm}$  (Pa) represents  
 145 the ambient pressure.  $K_s$  is set to 4000 as a constant following Oleson et al. (2010), to  
 146 limit photosynthesis of C<sub>4</sub> plants get saturated at lower CO<sub>2</sub> concentrations.

$$g_s = m \frac{(A_{tot} - R_d) \times RH}{c_s} + b \quad (5)$$

147 The stomatal conductance ( $g_s$ ),  $\text{mol [H}_2\text{O] m}^{-2} \text{ s}^{-1}$ ) is linked to the variations of  $A_{tot}$   
 148 with parameters such as dark respiration rate ( $R_d$ ),  $\text{umol m}^{-2} \text{ s}^{-1}$ ), relative humidity  
 149 ( $RH$ ), and CO<sub>2</sub> concentration at the leaf surface ( $c_s$ ). The model simulates the  
 150 biophysical processes of eight PFTs including tundra, C<sub>3</sub>/C<sub>4</sub> grass, shrubland, deciduous  
 151 broadleaf forest, evergreen broadleaf forest, evergreen needleleaf forest, and cropland.  
 152 Different values are assigned to parameters  $m$  and  $b$  for each PFT (Table S1). The  
 153 carbon uptake by the leaf is then accumulated and allocated to different organs to  
 154 support the plant development with dynamical changes in LAI and tree growth.

## 156 2.2 The O<sub>3</sub>-vegetation damage scheme

157 The YIBs model employs a semi-mechanistic parameterization proposed by Sitch  
 158 et al. (2007) to estimate the impact of O<sub>3</sub> on photosynthesis through stomatal uptake.  
 159 The scheme applies an undamaged factor ( $F$ ) ( $\text{nmol m}^{-2} \text{ s}^{-1}$ ) to both  $A_{tot}$  and  $g_s$  as  
 160 follows:

$$A_{totd} = A_{tot} \cdot F \quad (36)$$

$$g_{sd} = g_s \cdot F \quad (47)$$

161 where  $A_{totd}$  and  $g_{sd}$  are the unaffected photosynthesis and stomatal conductance  
 162 separately. The factor  $F$  is defined as:

$$F = 1 - a_h \cdot \max [F_{O_3} - F_{O_3,crit}, 0.0] \quad (58)$$

163  $a_h$  ( $\text{mmol m}^{-2} \text{ s}^{-1}$ ) is the high O<sub>3</sub> sensitivity coefficient, calibrated by Sitch et al. (2007)  
 164 on data from field observations by Karlsson et al. (2004) and Pleijel et al. (2004) to  
 165 represent ‘high’ sensitivity of relative species of each PFT.  $F_{O_3,crit}$  ( $\text{nmol m}^{-2} \text{ s}^{-1}$ ) is the  
 166 specific threshold for O<sub>3</sub> damages, both of which varies with vegetation types (Table  
 167 S1).

$$F_{O_3} = \frac{[O_3]}{R_a + \frac{k_{O_3}}{g_{sd}}}, \quad (69)$$

168 where  $[O_3]$  represents surface  $O_3$  concentrations,  $R_a$  ( $s\ m^{-1}$ ) stands for ~~the~~  
 169 aerodynamic ~~and boundary layer~~ resistance, which expresses turbulent transport  
 170 efficiency in transferring sensible heat and water vapor between the land surface and a  
 171 reference height. The constant  $k_{O_3}=1.67$  is the ratio of stomatal resistance for  $O_3$ ,  
 172 estimated based on the theoretical stomatal resistance to ~~that for water~~-water (Laisk et  
 173 al., 1989). When plants are exposed to  $[O_3]$  (Eq. 9),  $A_{tot}$  and  $g_s$  will decrease (Eq. 6  
 174 and Eq. 7) if the excess  $O_3$  enters leaves (Eq. 8). The increased stomatal resistance acts  
 175 to protect plants by reducing the  $O_3$  uptake of stomata. Consequently, the damage  
 176 scheme describes both changes in photosynthetic rate and stomatal conductance.

177

### 178 2.3 Experiments

179 To explore the coupled  $O_3$ -vegetation effect, we performed two ~~sets of~~ simulations  
 180 using the ModelE2-YIBs model. The control experiment “~~10NO3O3~~ offline” was  
 181 conducted without the  $O_3$  damages to vegetation. As a comparison, the sensitivity  
 182 experiment “~~10HO3O3~~ online” contained online  $O_3$ -vegetation interaction with high  
 183  $O_3$  sensitivity. For both experiments, the ~~2010s~~-anthropogenic emissions of 2010 (the  
 184 average of 2005-2014) for 8 species (BC, OC, CO,  $NH_3$ ,  $NO_x$ ,  $SO_2$ , Alkenes, and  
 185 Paraffin) from 8 economic sources (agriculture, energy, industry, transportation,  
 186 resident, solvent, waste, and international shipping) and biomass burning source were  
 187 collected from the Coupled Model Intercomparison Project phase 6 (CMIP6) (van  
 188 Marle et al., 2017; Hoesly et al., 2018). The ensemble mean of monthly sea surface  
 189 temperature (SST) and sea ice fraction (SIC) simulated by 21 CMIP6 models during  
 190 the time period 2005-2014 was employed as the boundary conditions. The cover  
 191 fraction of 8 PFTs (Fig. S1) fixed at 2010 were adopted from the land use harmonization  
 192 (LUH2) dataset (Hurtt et al., 2020). For each time-slice simulation, the model was run  
 193 for 30 years with all the input data fixed and the first 10 years are used as the spin up.  
 194 We calculated the average of the last 20 years and focused on the boreal summer season  
 195 (June-July-August, JJA) when the interaction of vegetation and surface  $O_3$  reaches the

196 maximum in one year- ([fig. S3](#)). [In order to show the uncertainty introduced by the](#)  
197 [internal variability of the model, all the related global/regional values are denoted as](#)  
198 [“mean/sum ± standard deviation of the last 20 model years”](#). We explored the climatic  
199 responses to O<sub>3</sub>-vegetation interactions as the differences between “~~10H~~[O<sub>3</sub>\\_online](#)”  
200 and “~~10N~~[O<sub>3</sub>\\_offline](#)” on the global scale with the ~~special~~ focus over the hotspot  
201 regions such as eastern U.S. (30–40° N, 80–90 ° W) and eastern China (22.5–38° N,  
202 106–122° E).

#### 204 **2.4 Data for ~~evaluations~~[model evaluation](#)**

205 We evaluated the simulated air pollutants, carbon fluxes, and meteorological  
206 variables [from ‘O<sub>3</sub>\\_offline’ run](#) using observational and reanalysis datasets. The  
207 worldwide observations of ~~O<sub>3</sub>~~[the maximum daily 8-hour average O<sub>3</sub> \(MDA8 O<sub>3</sub>\)](#)  
208 concentrations were [mainly](#) collected from three regional networks: Air Quality  
209 Monitoring Network operated by Ministry of Ecology and Environment (AQMN-MEE)  
210 in China, the Clean Air Status and Trends Network (CASTNET) in the U.S., and the  
211 European Monitoring and Evaluation Programme (EMEP) in Europe. ~~For the latter two~~  
212 ~~networks, we chose the average over 2009-2011, while for~~[Observations used for](#)  
213 [validation beyond China, sourced from Sofen et al. \(2016\), are averaged over the period](#)  
214 [2005-2014. This dataset encompasses 7288 station records worldwide and excludes the](#)  
215 [uncertainty associated with high mountain-top sites.](#) For AQMN-MEE, the mean value  
216 of 2014-2018 was used due to its establishment in 2013. The simulated aerosol optical  
217 depth (AOD) ~~was~~[and LAI were](#) validated using satellite-based data from the Moderate  
218 Resolution Imaging Spectroradiometer (MODIS) retrievals [collection 5](#) (Remer et al.,  
219 2005) (<http://modis.gsfc.nasa.gov/>) [averaged](#) for the years ~~2009-2011~~[2005-2014](#). The  
220 simulated GPP was evaluated against the data product upscaled from the FLUXNET  
221 eddy covariance measurements for 2009-2011 (Jung et al., ~~2009~~[2011](#)). The daily  
222 temperature at 2m (T<sub>2m</sub>) in ~~2009-2011~~[2005-2014](#) was obtained from the National  
223 Centers for Environmental Prediction/National Center for Atmospheric Research  
224 (NCEP/NCAR) reanalysis 1 (NCEP1) (Kalnay et al., 1996). For precipitation, we used  
225 the monthly data [averaged in 2005-2014](#) from Global Precipitation Climatology Project

(GPCP) (Huffman et al., 1997; Adler et al., 2018). All these datasets were interpolated to the same resolution as ModelE2-YIBs model. Normalized Root-mean-square-error (RMSE) and normalized mean biases (NMBs) were applied to quantify the deviations of simulations from observations ~~as follows:~~

$$RMSE = \sqrt{\frac{1}{n} \sum_{i=1}^n (S_i - O_i)^2} \quad (10)$$

$$NMB = \frac{\sum_{i=1}^n (S_i - O_i)}{\sum_{i=1}^n O_i} \times 100\% \quad (711)$$

$$-100\% NMB = \frac{\sum_{i=1}^n (S_i - O_i)}{\sum_{i=1}^n O_i} \times 100\%$$

Here,  $S_i$  and  $O_i$  represent the simulated and observed values, respectively.  $n$  denotes the total grid number used in the comparisons.

### 3. Results

#### 3.1 ~~Model~~ The control simulation and model evaluations

We first evaluated the air pollutants simulated by the control simulation O3 offline of ModelE2-YIBs model (Fig. 1). Over a total of ~~491~~503 grids with site-level  $O_3$  measurements (Fig. 1b), the model ~~adequately~~ replicated both the magnitude and spatial distribution of ~~the maximum daily 8-hour average (MDA8)  $O_3$  concentrations ( $\{O_3\}$ ),~~ with correlation coefficient ( $r$ ) of ~~0.58~~0.59 and NMB of ~~-1.27~~-1.54% (Fig. 1c). Simulated summertime surface  $\{MDA8 O_3\}$  was high in regions with large anthropogenic emissions, such as western Europe and eastern China (Ohara et al., 2007), as well as in central Africa with frequent fire emissions (van der Werf et al., 2017). On the global scale, the model yielded an average  $\{MDA8 O_3\}$  of ~~44.36~~43.93 ppbv and observations showed an average of ~~44.57~~42 ppbv over the same grids. However, the modeled result is overestimated over the North China Plain and slightly underestimated over the U.S., likely due to the biases in the emission inventories and predicted climate that drive the  $O_3$  production. Simulated AOD at 550 nm by O3 offline (Fig. 1d) showed similar spatial pattern as the satellite retrievals (Fig. 1e) with ~~a high~~  $R=0.770.75 and ~~low~~ NMB of ~~-6.27~~-7.35% globally (Fig. 1f). Both the simulations and observations showed AOD hotspots over North Africa and the Middle East where dust emissions dominate, and in$

252 northern India and eastern China where anthropogenic emissions are large- ([Feng et al.,](#)  
253 [2020](#)).

254 We then evaluated the simulated GPP and LAI [by the control experiment](#) for the  
255 boreal summer period (Fig. 2). Observations showed GPP hotspots over boreal forests  
256 such as eastern U.S., Eurasia, and East Asia and the tropical forests such as Amazon,  
257 central Africa, and Indonesia (Fig. 2b). The seasonal total GPP was estimated to be  
258 41.63Pg[C], which accounted for 35% of the annual amount. Simulations ~~well~~ captured  
259 the observed GPP pattern on the global scale, with  $r = 0.6364$  and  $NMB = -12.447.81\%$   
260 over 2581 grids (Fig. 2c), with underestimation in the tundra area and slight  
261 overestimation in the tropical rain forest and evergreen forest regions. The model  
262 simulated a seasonal total GPP of ~~36.45~~[38.69](#) Pg[C], equivalent to 34% of the annual  
263 amount. Simulated LAI showed similar patterns as GPP (Fig. 2d) and resembled  
264 observed LAI (Fig. 2e) with a ~~high~~ spatial correlation  $r = 0.79$  and a low  $NMB = -$   
265 ~~5.19~~[43](#)% over 4435 grids globally (Fig. 2f).

266 We further validated the simulated meteorology [from O3 offline](#) (Fig. S2). For  
267 [surface air](#) temperature, the model (Fig. S2a) reproduced observed (Fig. S2b) pattern  
268 with ~~low NMB~~[RMSE](#) of ~~8.49%~~[3.21 °C](#) and ~~high~~  $r$  of 0.99 against observations (Fig.  
269 S2c). For precipitation, ~~both simulations~~[the simulation](#) (Fig. S2d) ~~and~~  
270 ~~observations~~[captures the observed spatial pattern](#) (Fig. S2e) ~~showed high values in the~~  
271 ~~tropical oceans~~ with  $NMB = 16.91[17.26](#)% and  $r = 0.74$  ~~between them~~[75](#) (Fig. S2f).  
272 Overall, the model ~~showed good performance in the simulations~~[captures the spatial](#)  
273 [characteristics and magnitudes](#) of air pollutants, biospheric parameters, and  
274 meteorological fields, ~~and provided~~[making it a useful](#)[valuable](#) tool for studying ~~the~~ O<sub>3</sub>-  
275 vegetation interactions.$

### 277 3.2 O<sub>3</sub> damage to terrestrial ecosystems

278 We assessed the damaging effects of surface O<sub>3</sub> to ecosystems (~~Fig. due to online~~  
279 [O<sub>3</sub>-vegetation interactions](#) (Fig. 3). The impacts of O<sub>3</sub> on biospheric variables were  
280 mainly located in regions characterized by abundant vegetation cover and elevated O<sub>3</sub>  
281 concentrations. On the global scale, O<sub>3</sub> induced the GPP reduction of ~~-1.80±~~[0.8761](#) PgC

282 yr<sup>-1</sup> (~~-3.09~~4.69±1.56%, Fig. 3a). This deleterious effect was more pronounced in  
283 specific regions, notably eastern China and eastern U.S., with significant GPP declines  
284 of ~~-18.43~~25.40±1.90% and ~~-16.12~~20.14±5.02%, respectively, under high O<sub>3</sub> sensitivity  
285 conditions (Fig. 3a and Table S2). Meanwhile, stomatal conductance significantly  
286 decreased in the middle latitudes of Northern Hemisphere (Fig. 3b). The most  
287 substantial relative change of -30.62±4.30% was observed in eastern China, followed  
288 by -25.65±9.32% in the eastern U.S. (Fig. 3b and Table S2). Though there are positive  
289 responses in some regions, they are not dominant and hardly significant. These values  
290 were stronger than that for GPP (Fig. 3a), likely due to the climatic feedback to O<sub>3</sub>-  
291 vegetation interactions. The opening of plant stoma plays a crucial role in regulating  
292 the energy and water exchange between land surface and the atmosphere. The inhibition  
293 of stomatal conductance by surface O<sub>3</sub> leads to the warmer (Fig. 4a) and drier (Fig. 4b)  
294 climate in those hotspot regions, resulting in even stronger inhibition effects on stomatal  
295 conductance. Following the changes in GPP, global LAI on average decreased by  
296 0.01±0.01 m<sup>2</sup> m<sup>-2</sup> (-0.62±0.84%) with regional maximums of -4.53±1.14% in eastern  
297 China and -5.87±3.11% in eastern U.S. (Table S2).

### 299 3.3 Global climatic responses to O<sub>3</sub>-vegetation interactions

300 In response to the O<sub>3</sub>-induced inhibition of stomatal conductance, surface air  
301 temperature increased by ~~0.05~~0.05±0.20°C (Fig. 4a) while precipitation decreased by  
302 -0.01±0.03 mm day<sup>-1</sup> (Fig. 4b) on the global scale. The most significant change was the  
303 warming of 0.56±0.38°C and precipitation reduction of -0.79±1.05 mm day<sup>-1</sup> (  
304 16.18±20.38%) in eastern China (Table S3), following the largest inhibition to stomatal  
305 conductance (Fig. 3b). Such warming and rainfall deficit also appeared in eastern U.S.  
306 and western Europe, where the O<sub>3</sub>-vegetation interactions were notable. The O<sub>3</sub>-  
307 induced inhibition to stomatal conductance decreased latent heat flux (Fig. 4e) and the  
308 consequent precipitation (Fig. 4b) in those hotspot regions. Meanwhile, the reduction  
309 of latent heat flux promotes surface air temperature (Fig. 4a), resulting in the increase  
310 of sensible heat flux (Fig. 4f). Such warming was also reported in field experiments,

311 where relatively high O<sub>3</sub> exposure resulted in noticeable increases of canopy  
312 temperature along with reductions of transpiration (Bernacchi et al., 2011; VanLoocke  
313 et al., 2012). Globally, temperature and precipitation showed patchy responses with  
314 both positive and negative anomalies, suggesting that the regional hotspots of O<sub>3</sub>-  
315 induced meteorological changes propagate to surrounding areas through atmospheric  
316 perturbations.

317 We further examined the changes in air humidity and cloudiness. Surface relative  
318 humidity decreased by  $-0.18 \pm 0.53\%$  globally with a similar pattern as that of  
319 precipitation (Fig. 4c). The most significant reductions were over eastern China and  
320 eastern U.S., where both the warming (Fig. 4a) and rainfall deficit (Fig. 4b) contributed  
321 to the drought. However, in the adjacent regions such as northern China and central  
322 U.S., both rainfall and surface relative humidity showed certain enhancement. These  
323 changes were associated with the regional increase of cloud cover (Fig. 4d). The  
324 sensible heat flux increased by  $6.3 \pm 5.4$  W m<sup>-2</sup> ( $16.54 \pm 15.59\%$ ) and  $7.12 \pm 3.86$  W m<sup>-2</sup>  
325 ( $25.46 \pm 14.71\%$ ) in eastern U.S. and eastern China, respectively, suggesting a transfer  
326 of thermal energy from land to the atmosphere by O<sub>3</sub>-vegetation interactions (Fig. 4f  
327 and Table S3). The warming effect further triggered anomalous updrafts in the lower  
328 troposphere, represented by the changes in vertical velocity (Fig. 5), leading to  
329 enhanced convection, reduced atmospheric stability, and consequently an increase in  
330 low-level cloudiness (Fig. 4d). However, despite the usual cooling effect associated  
331 with increased cloud cover due to reductions in radiation, in regions predominantly  
332 influenced by O<sub>3</sub>-vegetation interactions, this cooling effect was outweighed by the O<sub>3</sub>-  
333 induced warming through inhibition of stomatal conductance. Therefore, temperatures  
334 exhibited an overall increase of  $0.56 \pm 0.38$  °C in eastern China and  $0.33 \pm 0.87$  °C in the  
335 eastern U.S. (Table S3).

### 337 **3.4 Changes of air pollution by O<sub>3</sub>-vegetation interactions**

338 Changes in surface water and heat fluxes induced by O<sub>3</sub>-vegetation interactions  
339 could feed back to affect air pollutants such as O<sub>3</sub> and aerosols. As Fig. 6a and Table  
340 S4 show, surface MDA8 O<sub>3</sub> concentrations enhanced  $1.26 \pm 3.02$  ppbv in eastern

341 China and  $0.981.15 \pm 1.77$  ppbv in eastern U.S. due to the decreased dry deposition  
342 following O<sub>3</sub> inhibition on stomatal conductance. It indicates that the high  
343 contemporary O<sub>3</sub> pollution may worsen air quality through O<sub>3</sub>-vegetation interactions.  
344 However, negative O<sub>3</sub> changes were predicted in central U.S. and western China, where  
345 the increased rainfall dampened O<sub>3</sub> through chemical reactions and wet deposition. On  
346 a global scale, surface MDA8 O<sub>3</sub> showed a limited increase of  $0.0203 \pm 0.4$  ppbv due to  
347 the offset between positive and negative feedbacks. The enhancement of O<sub>3</sub>  
348 concentrations in polluted regions may exacerbate the warming effect of O<sub>3</sub> as a  
349 greenhouse gas and cause additional damages to vegetation. For instance, offline O<sub>3</sub>  
350 damages on GPP in eastern China and the eastern US are  $-0.52 \pm 0.03$  Pg[C] ( $-$   
351  $24.98 \pm 0.91\%$ ) and  $-0.17 \pm 0.02$  Pg[C] ( $-16.71 \pm 1.16\%$ ), respectively, smaller than those  
352 induced by O<sub>3</sub>-vegetation interactions (Table S2).

353 Aerosols also exhibited evident changes by the O<sub>3</sub>-vegetation interactions. The  
354 AOD showed significant reductions over the hotspot regions such as eastern China and  
355 eastern U.S. (Fig. 6b). In the ModelE2-YIBs model, sulfate was especially sensitive to  
356 cloud which could enhance the aerosol scavenging through cloud water precipitation  
357 (Koch et al., 2006). The large enhancement of cloudiness removed sulfate more  
358 efficiently than other aerosol species, leading to an average decline of  $-1.94 \pm 1.67$   $\mu\text{g}$   
359  $\text{m}^{-3}$  ( $-8.52 \pm 6.88\%$ ) in PM<sub>2.5</sub> loading over eastern China (Fig. ~~S3~~S4 and Table S4).  
360 Meanwhile, the reduction of surface relative humidity (Fig. 4c) in the regions with  
361 strong O<sub>3</sub>-vegetation interactions limited the hygroscopic growth of aerosols, leading  
362 to a more noticeable decrease in AOD (Petters and Kreidenweis, 2007; ~~Revised~~  
363 ~~algorithm for estimating light extinction from IMPROVE particle speciation data,~~  
364 ~~2023~~Pitchford et al., 2007) by  $-0.06 \pm 0.05$  ( $-14.67 \pm 16.75\%$ ) in eastern China (Table S4).  
365 The similar aerosol changes were found in eastern U.S. but with smaller reductions of  
366 PM<sub>2.5</sub> by  $-0.27 \pm 0.36$   $\mu\text{g}$   $\text{m}^{-3}$  ( $-6.01 \pm 7.9\%$ ) and AOD by  $-0.01 \pm 0.01$  ( $-8.2515 \pm 9.38\%$ )  
367 (Table S4). Beyond the key O<sub>3</sub>-vegetation coupling regions, positive but insignificant  
368 changes in AOD were predicted, leading to the moderate AOD changes on the global  
369 scale (Fig. 6b).

370

#### 371 4. ~~Conclusions~~Discussion and ~~discussion~~conclusions

372 We examined the O<sub>3</sub>-vegetation feedback to climate and air pollution in the 2010s  
373 using the fully coupled climate-carbon-chemistry model ModelE2-YIBs. During boreal  
374 summer, surface O<sub>3</sub> resulted in strong damages to GPP and inhibitions to stomatal  
375 conductance with regional hotspots over eastern China and eastern U.S. Consequently,  
376 surface transpiration was weakened, leading to decreased latent heat fluxes and relative  
377 humidity but increased surface air temperature. Meanwhile, the surface warming  
378 increased cloud cover by reducing atmospheric stability. ~~The~~However, the  
379 enhancement of cloudiness ~~further~~ decreased surface temperature and promoted  
380 precipitation ~~nearby~~outside the key regions with intense O<sub>3</sub>-vegetation interactions. The  
381 O<sub>3</sub>-induced inhibition to stomatal conductance resulted in a localized increase in O<sub>3</sub>  
382 concentrations. In contrast, the increased cloud cover and decreased relative humidity  
383 jointly reduced AOD in hotspot regions. On the global scale, the mean changes of both  
384 climate and air pollution were moderate due to the offset between the changes with  
385 opposite signs.

386 Our predicted changes in water/heat fluxes by O<sub>3</sub>-vegetation interactions were  
387 consistent with previous studies (Lombardozzi et al., 2015; Arnold et al., 2018; Gong  
388 et al., 2020). For example, the simulations by Lombardozzi et al. (2015) revealed that  
389 surface O<sub>3</sub> reduces global GPP by 8%-12% and transpiration by 2-2.4% with regional  
390 reductions up to 20% for GPP and 15% for transpiration in eastern China and U.S.  
391 These changes were in general consistent with our results though we predicted larger  
392 reductions in transpiration than GPP due to O<sub>3</sub>-vegetation interactions. Using the same  
393 scheme as Lombardozzi et al. (2015), Sadiq et al. (2017) showed that O<sub>3</sub>-vegetation  
394 coupling induced the surface warming of 0.5-1°C and O<sub>3</sub> enhancement of 4-6 ppbv in  
395 eastern China and eastern U.S. The magnitude of these responses was much stronger  
396 than our predictions, likely because they considered the accumulation effect of O<sub>3</sub>. In  
397 contrast, the regional simulations by Jin et al. (2023) revealed that O<sub>3</sub>-vegetation  
398 coupling led to the increases of temperature up to 0.16°C and surface O<sub>3</sub> up to 0.6 ppbv  
399 in eastern China, both of which were smaller than our predictions. The damage scheme

400 they use, which depends on cumulative O<sub>3</sub> uptake, omits the difference in impact on  
401 sunlit or shaded leaves and will overestimate the O<sub>3</sub> damage on GPP compared to the  
402 scheme we use, which considers transient O<sub>3</sub> flux (Cao et al., [2023](#)[2024](#)). The  
403 discrepancies of O<sub>3</sub>-vegetation feedback using the same O<sub>3</sub> damage schemes revealed  
404 the uncertainties from climate and chemistry models. Our predictions were within the  
405 range of previous estimates for both climatic and O<sub>3</sub> changes.

406 There were some limitations in our simulated O<sub>3</sub>-vegetation interactions. First, the  
407 semi-mechanistic O<sub>3</sub> damage scheme we used in the study linked the damages to  
408 photosynthesis with those to stomatal conductance (Sitch et al., 2007), leading to  
409 stronger inhibition percentage in stomatal conductance than that in photosynthesis  
410 considering the O<sub>3</sub>-vegetation feedback. However, some observations showed that the  
411 damage to stomatal conductance occurred more slowly and might not be proportional  
412 to the decline of photosynthetic rates (Gregg et al., 2006; Lombardozzi et al., 2012).  
413 Second, observations have shown large variability of plant sensitivities to O<sub>3</sub> damages.  
414 The Sitch et al. (2007) scheme employed the low to high ranges of sensitivity to indicate  
415 the inter-specific variabilities. In this study, we employed only the high O<sub>3</sub> sensitivity  
416 to explore the maximum responses. The possible uncertainties due to varied O<sub>3</sub> damage  
417 sensitivities deserved further investigations. Third, large-scale observations were not  
418 available to validate the simulated regional to global responses of climate and air  
419 pollutants. The O<sub>3</sub> vegetation damage scheme was extensively validated against site-  
420 level measurements of both photosynthesis (Yue and Unger, 2018) and stomatal  
421 conductance (Yue et al., 2016). However, we were conservative about the derived  
422 global responses given that previous studies showed large discrepancies using the same  
423 O<sub>3</sub> damage scheme but implemented in different climate and/or chemistry models  
424 (Lombardozzi et al., 2015; Sadiq et al., 2017; Jin et al., 2023). Furthermore, the 2°×2.5°  
425 resolution of current ModelE2-YIBs has limitation due to the high computational  
426 demands. ~~Ito et al. (2020) shows that the ModelE2.1 with fixed vegetation traits~~  
427 ~~reproduces carbon fluxes well, and that the model results are involved in the CMIP6~~  
428 ~~Coupled Climate Carbon Cycle MIP (C4MIP).~~ However, ~~analysis of the climate model~~  
429 ~~shows that~~ high-resolution ~~exhibits~~[models exhibit](#) improved simulations of extreme

430 events (Chang et al., 2020; Ban et al., 2021), ~~and the application of~~which have certain  
431 effect on O<sub>3</sub>-vegetation interactions (Mills et al., 2016; Lin et al., 2020). While chemical  
432 transport ~~model shows that~~models with relatively coarse resolution can raise biases in  
433 simulated air pollutants, ~~though it captures the~~they still capture large-scale ~~general~~  
434 ~~pattern almost the same as~~patterns similar to fine-resolution results and is reasonable ~~as~~  
435 compared to observational data (Wang et al., 2013; Li et al., 2016; Lei et al., 2020).  
436 Moreover, we omit the slow climatic feedback caused by air-sea interaction in the  
437 simulations. Studies have revealed that these interactions may result in different  
438 climatic perturbations from those simulations with fast responses of land surface alone  
439 (Yue et al., 2011). A dynamic ocean model is considered to enrich the future research.  
440 Meanwhile, this study does not isolate the different impacts of aerosols, even though  
441 the radiation module includes both direct and indirect radiative effects. We will  
442 investigate this further in the future by identifying the main processes.

443         Despite these uncertainties, our simulations revealed considerable changes of both  
444 climate and air pollutants in response to O<sub>3</sub>-vegetation interactions. The most intense  
445 warming, dryness, and O<sub>3</sub> enhancement were predicted in eastern China and eastern  
446 U.S., affecting the regional climate and threatening public health for these top two  
447 economic centers. In contrast, we for the first time revealed the reduction of aerosol  
448 loading in those hotspot regions, suggesting both positive and negative effects to air  
449 pollutants by O<sub>3</sub>-vegetation feedback. Such interactions should be considered in the  
450 Earth system models so as to better project future changes in climate and air pollutants  
451 following the anthropogenic interventions to both O<sub>3</sub> precursor emissions and  
452 ecosystem functions.

453

454 **Data Availability**

455 The observational data and model outputs that support the findings in this study are  
456 available from corresponding authors upon reasonable request.

457

458 **Author contributions**

459 XY conceived the project. XZ performed the model simulations, conducted results  
460 analysis and wrote the draft manuscript. XY, CT and XL assisted in the interpretation  
461 of the results and contributed to the discussion and improvement of the paper.

462

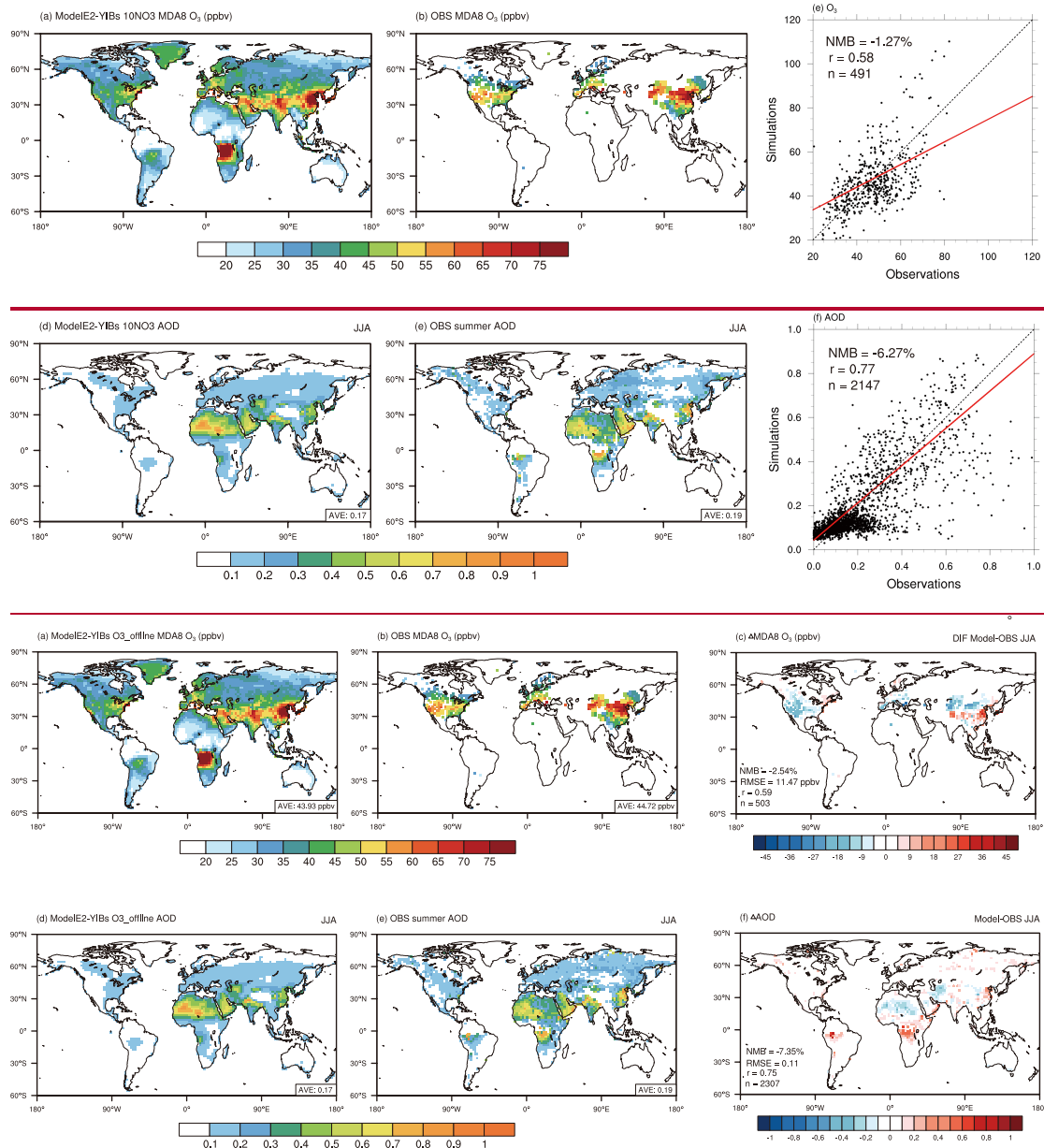
463 **Competing interests**

464 The authors declare that they have no conflict of interest.

465

466 **Acknowledgments**

467 This study was jointly funded by ~~the National Natural Science Foundation of China (no.~~  
468 ~~42293323)~~ and ~~National~~ National Key Research and Development Program of China  
469 (no. ~~2023YFF0805402~~2023YFF0805404) and National Natural Science Foundation of  
470 China (no. 42293323).

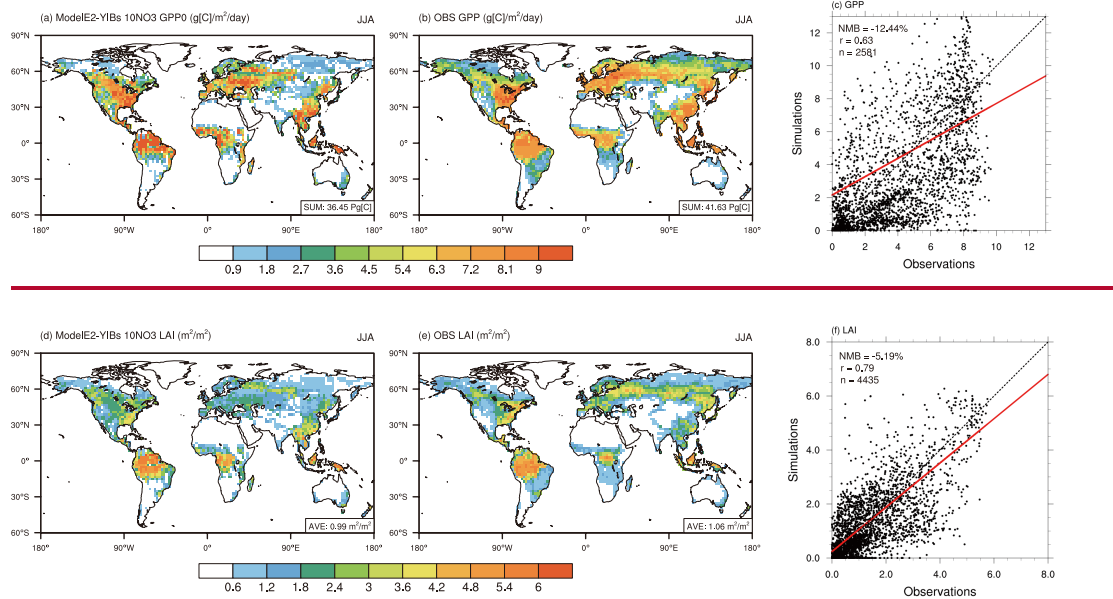


471

472

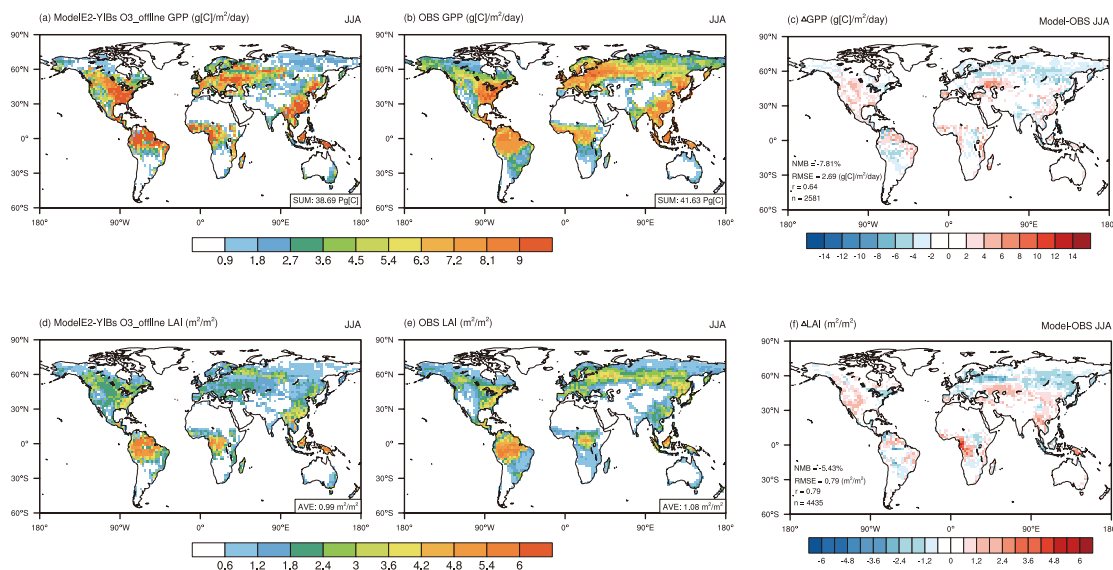
473 **Figure 1.** Evaluation of the boreal summertime (June-August) air pollutants **in 2010** at  
 474 **the present day** simulated by the ModelE2-YIBs model. Surface daily maximum 8-hour  
 475 ozone (MDA8 O<sub>3</sub>, **upper; a-c**) and aerosol optical depth (AOD, **bottom; d-f**) from the  
 476 simulation **10NO3** (**left O3 offline (a & d)**) and observations (**middle b & e**) are  
 477 compared. The correlation coefficients (r), **root mean square error (RMSE)**, normalized  
 478 mean bias (NMB), and number of grid cells (n) for the comparisons are listed on the  
 479 **scatter plots (e & f)**. The dashed line denotes the 1 : 1 ratio. The red line is the linear  
 480 **regression between the simulation and observation**. **mean bias maps (c & f)**.

481



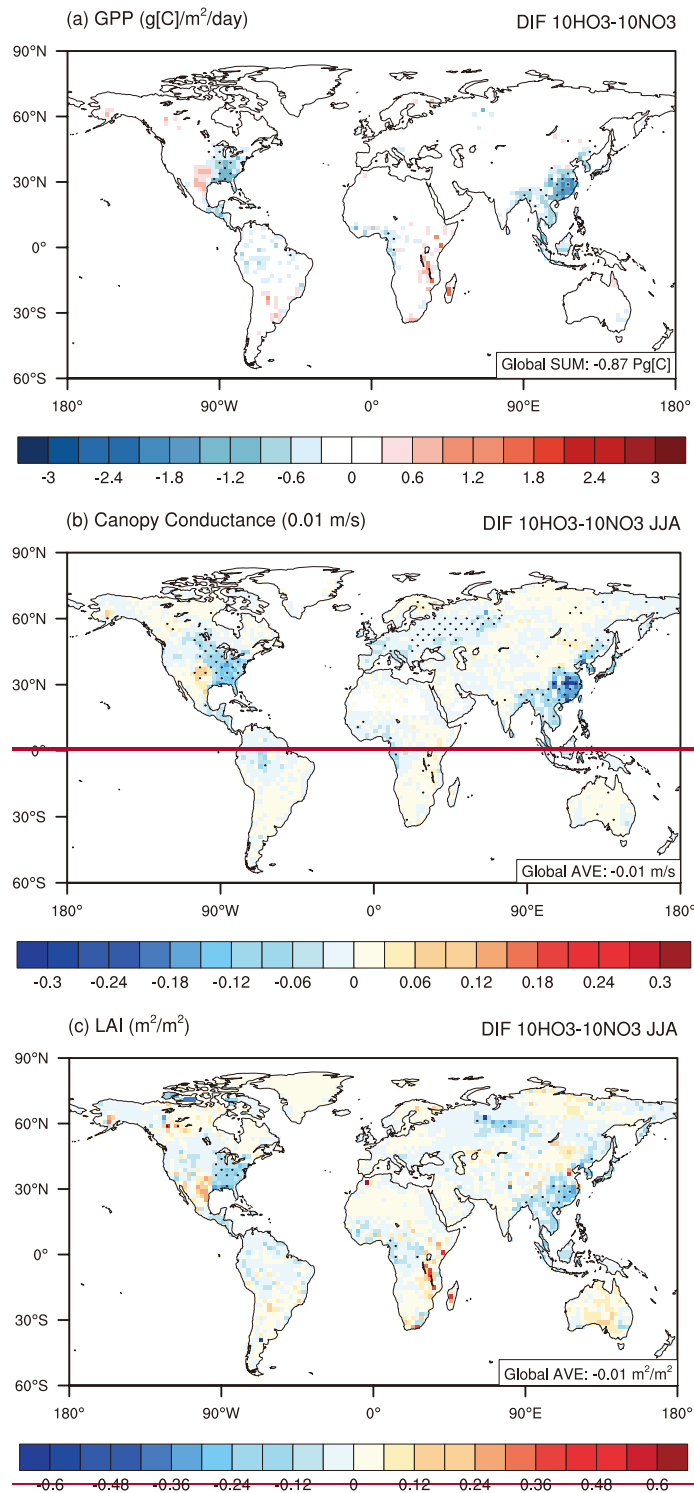
482

483

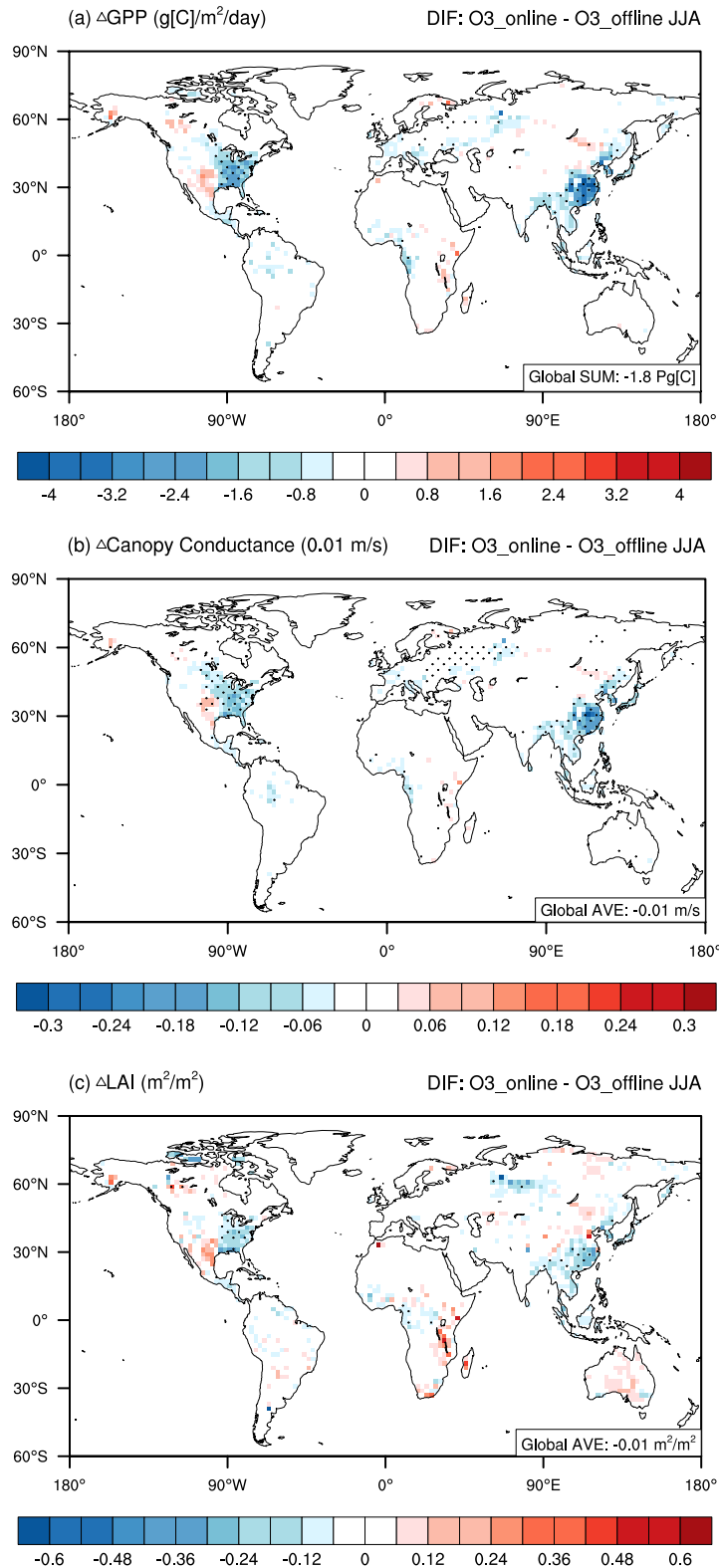


484

485 **Figure 2.** The same as Fig.1 but for gross primary productivity (GPP, upper panels; a-  
 486 c) and leaf area index (LAI, bottom panels; d-f).

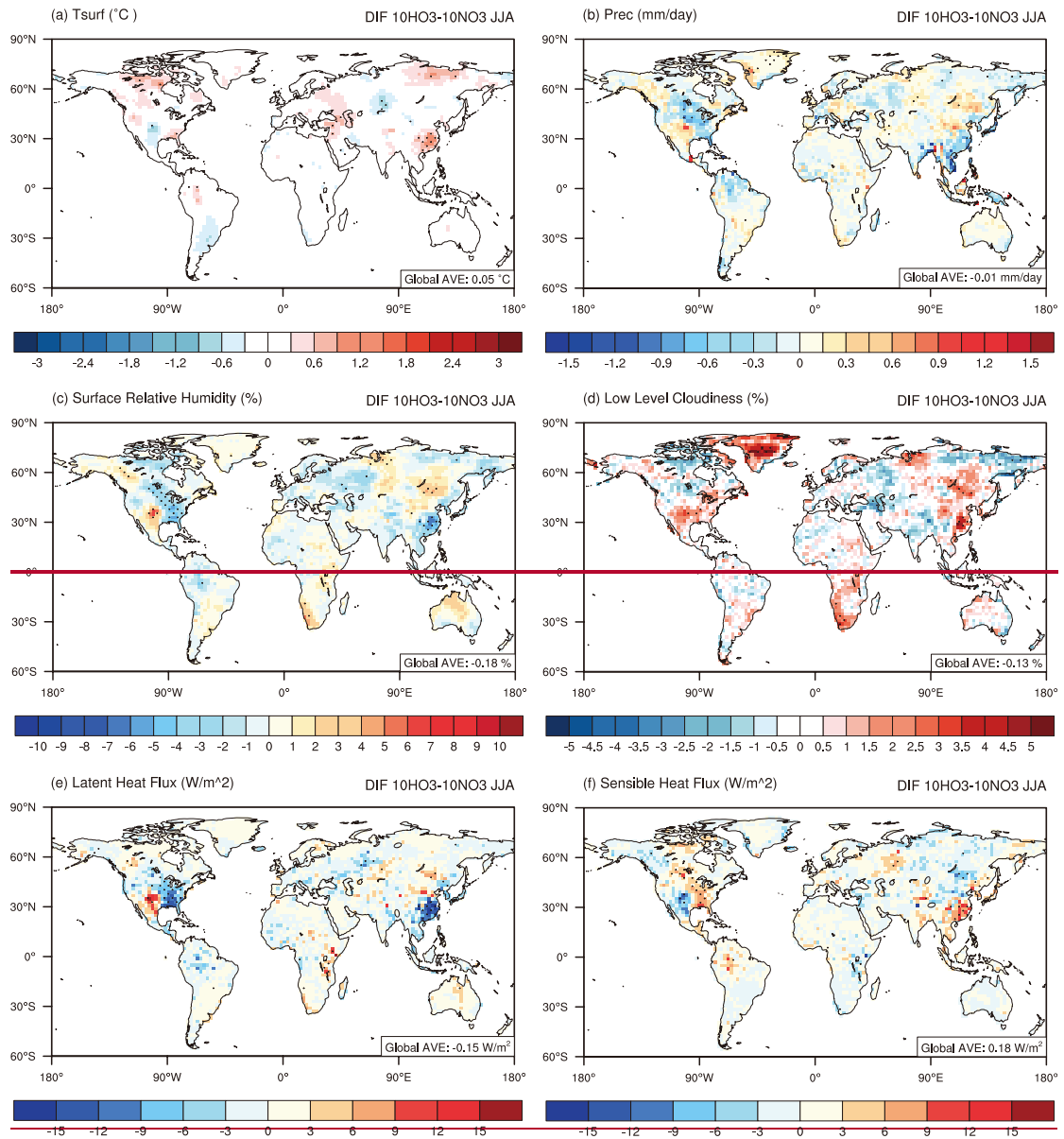


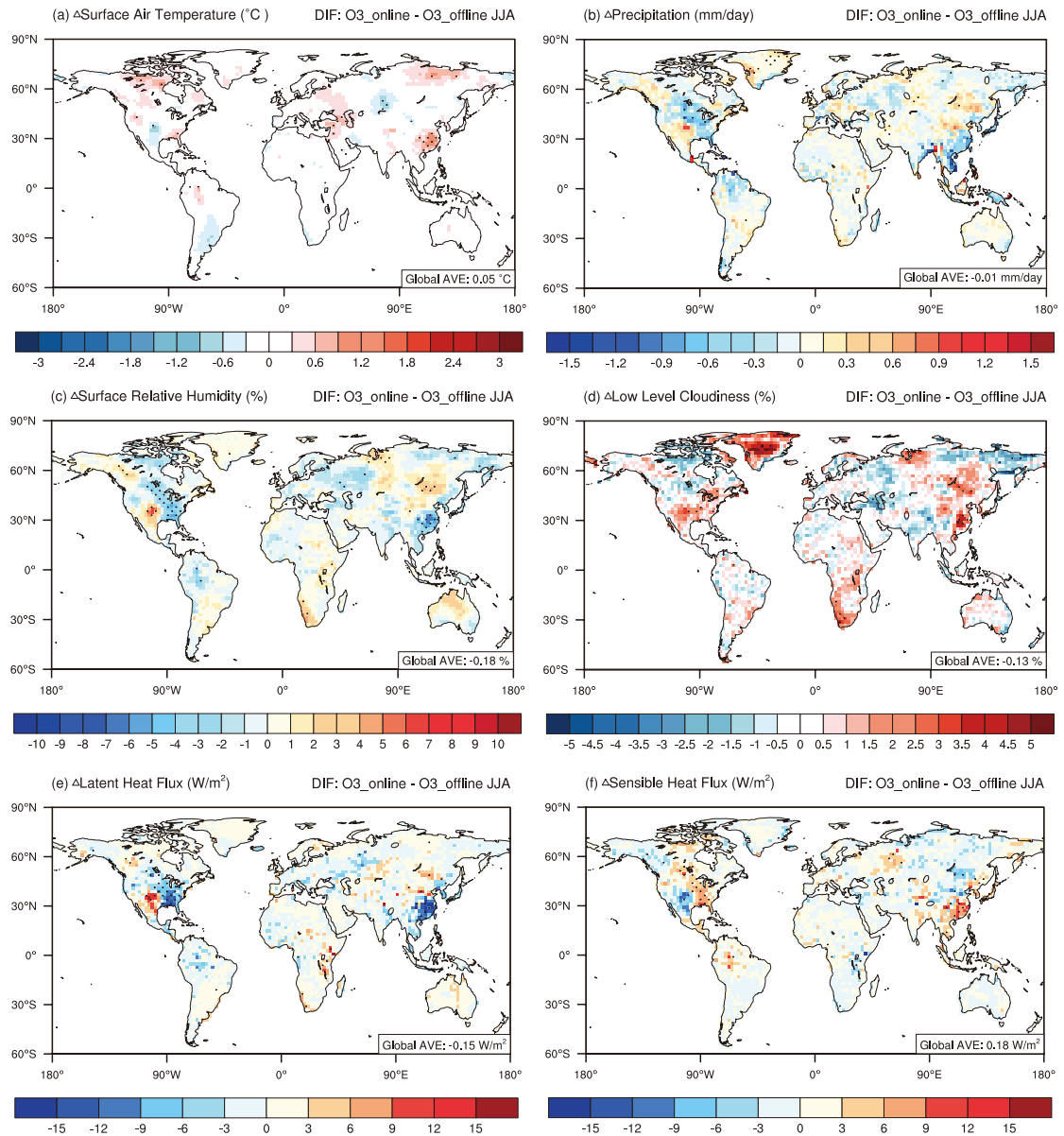
487



488

489 **Figure 3.** Changes of boreal summertime biospheric variables induced by O<sub>3</sub>-damages  
 490 in 2010s.-vegetation interactions at the present day. Results shown are changes of (a)  
 491 GPP, (b) canopy conductance, and (c) LAI between simulations 10H03O3\_online and  
 492 10N03O3\_offline. Black dots denote areas with significant changes ( $p < 0.1$ ). **Please**  
 493 **notice the differences in the color scales.**

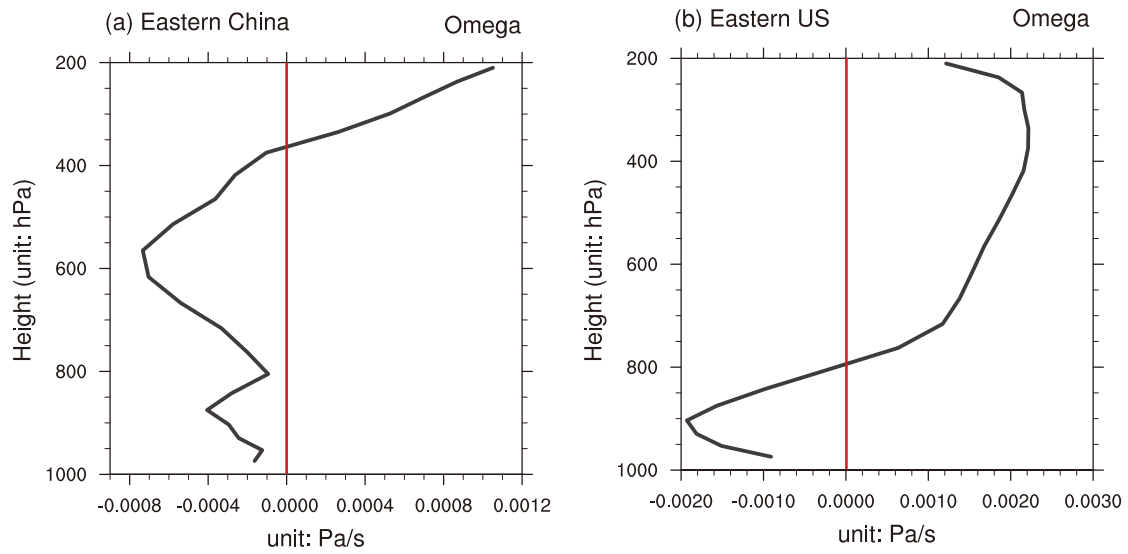




495

496 **Figure 4.** Changes of boreal summertime meteorological fields by ~~ozone~~ $O_3$ -vegetation  
 497 interactions ~~in 2010s~~at the present day. Results shown are changes of (a) surface air  
 498 temperature, (b) precipitation, (c) surface relative humidity, (d) low level cloudiness,  
 499 (e) latent heat flux, and (f) sensible heat flux between simulations ~~10H03~~ $O_3$  online  
 500 and ~~10N03~~ $O_3$  offline. For heat fluxes, positive values (shaded in red color) indicate  
 501 the upward fluxes change. Black dots denote areas with significant changes ( $p < 0.1$ ).  
 502 Please notice the differences in the color scales.

503



504

505

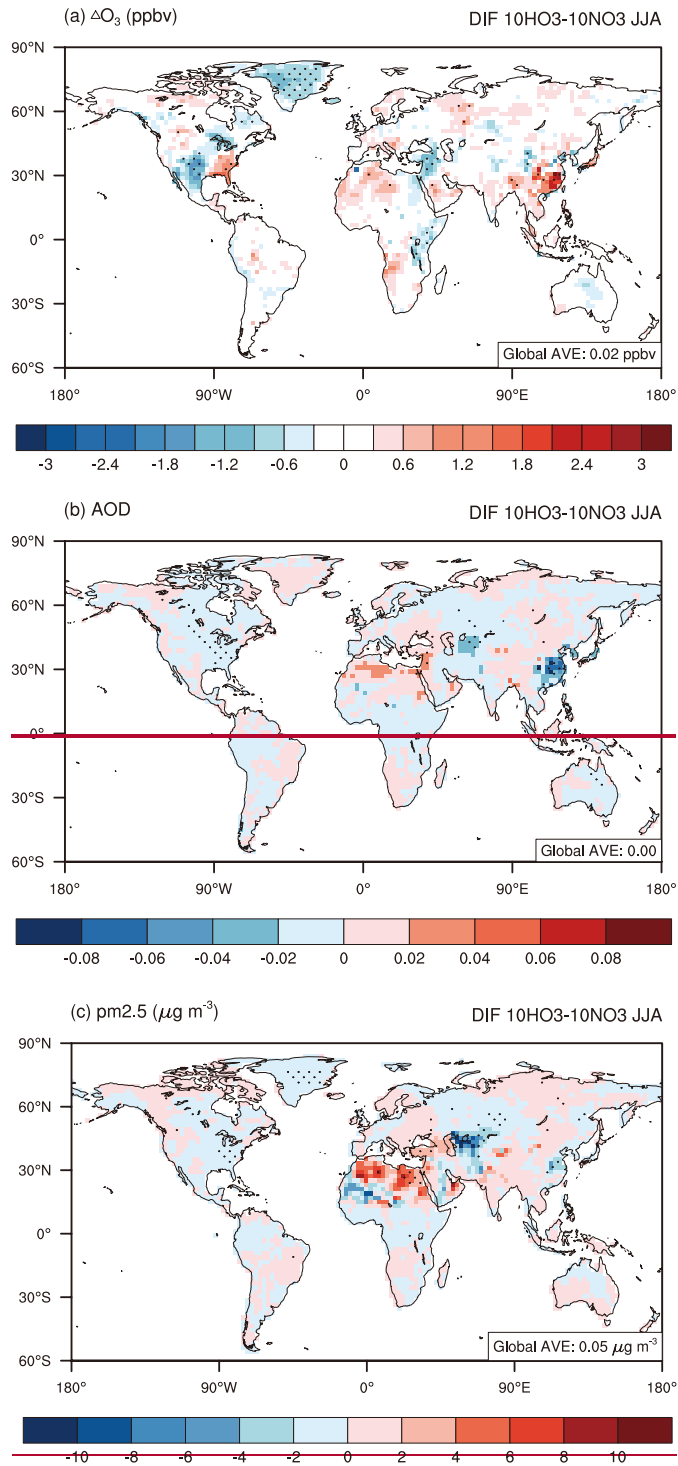
506

507

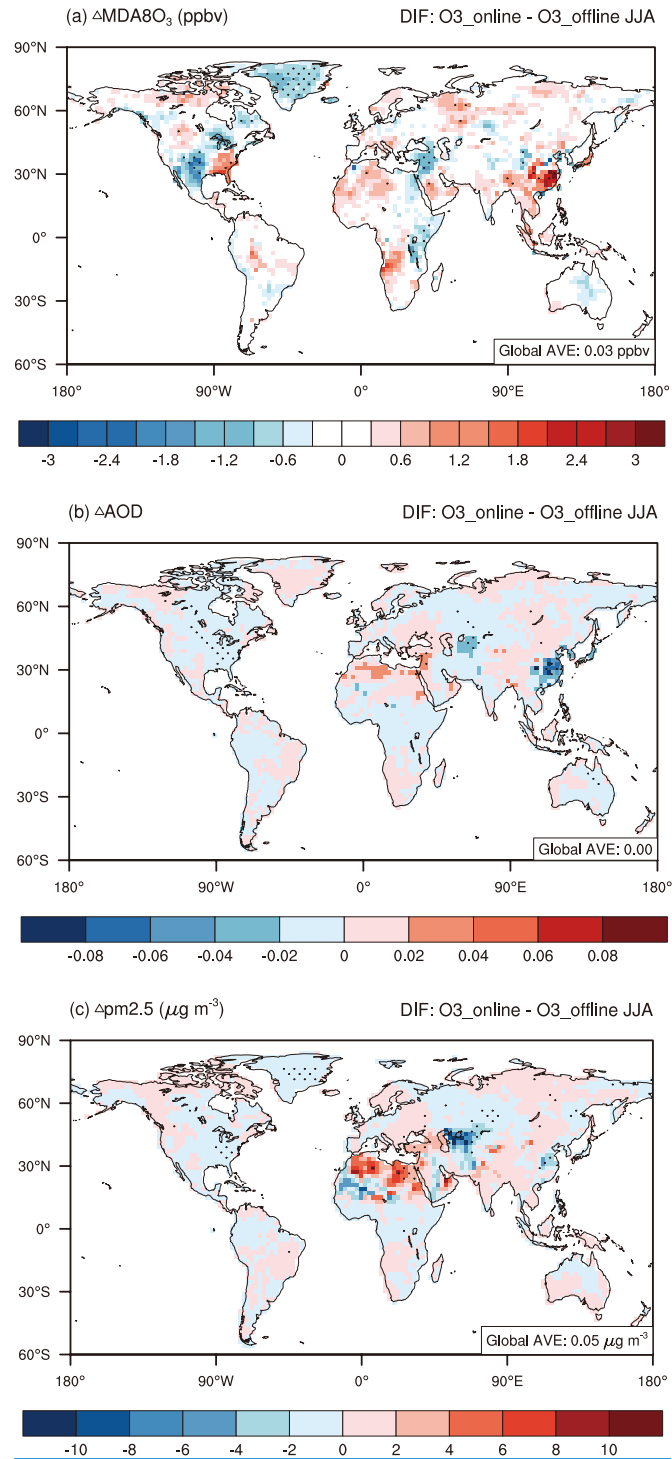
508

509

**Figure 5.** Vertical profile of vertical velocity. Results shown are changes of the vertical velocity in (a) Eastern China and (b) Eastern US between simulations ~~10H03O3~~[10H03O3\\_online](#) and ~~10N03O3~~[10N03O3\\_offline](#). Solid red line denotes the value 0. Please notice the differences in the scales.



510



511

512 **Fig. 6.** Changes of summertime atmospheric pollution caused by ~~ozone~~ $\text{O}_3$ -vegetation  
 513 interactions ~~in 2010s~~ at present day. Results shown are changes of (a) ~~ozone~~ $\text{O}_3$ , (b)  
 514 AOD, and (c)  $\text{PM}_{2.5}$  between ~~10H03~~ $\text{O}_3_{\text{online}}$  and ~~10N03~~ $\text{O}_3_{\text{offline}}$ . Black dots  
 515 denote areas with significant changes ( $p < 0.1$ ). ~~Please notice the differences in the color~~  
 516 ~~scales.~~

517

518 **References**

- 519 Adler, R. F., Sapiano, M. R. P., Huffman, G. J., Wang, J.-J., Gu, G., Bolvin, D., Chiu,  
520 L., Schneider, U., Becker, A., Nelkin, E., Xie, P., Ferraro, R., and Shin, D.-B.: The  
521 Global Precipitation Climatology Project (GPCP) Monthly Analysis (New Version  
522 2.3) and a Review of 2017 Global Precipitation, *Atmosphere*, 9, 138,  
523 <https://doi.org/10.3390/atmos9040138>, 2018.
- 524 Ainsworth, E. A., Yendrek, C. R., Sitch, S., Collins, W. J., and Emberson, L. D.: The  
525 effects of tropospheric ozone on net primary productivity and implications for  
526 climate change, *Annu. Rev. Plant. Biol.*, 63, 637–661,  
527 <https://doi.org/10.1146/annurev-arplant-042110-103829>, 2012.
- 528 Anav, A., Menut, L., Khvorostyanov, D., and Viovy, N.: Impact of tropospheric ozone  
529 on the Euro-Mediterranean vegetation, *Glob. Change. Biol.*, 17, 2342–2359,  
530 <https://doi.org/10.1111/j.1365-2486.2010.02387.x>, 2011.
- 531 Arnold, S. R., Lombardozzi, D., Lamarque, J. -F., Richardson, T., Emmons, L. K.,  
532 Tilmes, S., Sitch, S. A., Folberth, G., Hollaway, M. J., and Val Martin, M.:  
533 Simulated Global Climate Response to Tropospheric Ozone-Induced Changes in  
534 Plant Transpiration, *Geophys. Res. Lett.*, 45, 13070–13079,  
535 <https://doi.org/10.1029/2018GL079938>, 2018.
- 536 Ball, J. T., Woodrow, I. E., and Berry, J. A.: A Model Predicting Stomatal Conductance  
537 and its Contribution to the Control of Photosynthesis under Different  
538 Environmental Conditions, in: *Progress in Photosynthesis Research*, edited by:  
539 Biggins, J., Springer Netherlands, Dordrecht, 221–224,  
540 [https://doi.org/10.1007/978-94-017-0519-6\\_48](https://doi.org/10.1007/978-94-017-0519-6_48), 1987.
- 541 Ban, N., Caillaud, C., Coppola, E., Pichelli, E., Sobolowski, S., Adinolfi, M., Ahrens,  
542 B., Alias, A., Anders, I., Bastin, S. and Belušić, D.: The first multi-model ensemble  
543 of regional climate simulations at kilometer-scale resolution, part I: evaluation of  
544 precipitation, *Clim. Dynam.*, 57, 275-302, [https://doi.org/10.1007/s00382-021-](https://doi.org/10.1007/s00382-021-05708-w)  
545 [05708-w](https://doi.org/10.1007/s00382-021-05708-w), 2021.
- 546 [Buker, P., Feng, Z., Uddling, J., Briolat, A., Alonso, R., Braun, S., Elvira, S., Gerosa,](#)  
547 [G., Karlsson, P. E., Le Thiec, D., Marzuoli, R., Mills, G., Oksanen, E., Wieser, G.,](#)  
548 [Wilkinson, M., and Emberson, L. D.: New flux based dose-response relationships](#)  
549 [for ozone for European forest tree species, \*Environ. Pollut.\*, 206, 163–174,](#)  
550 <https://doi.org/10.1016/j.envpol.2015.06.033>, 2015.
- 551 Bernacchi, C. J., Leakey, A. D. B., Kimball, B. A., and Ort, D. R.: Growth of soybean  
552 at future tropospheric ozone concentrations decreases canopy evapotranspiration  
553 and soil water depletion, *Environ. Pollut.*, 159, 1464–1472,  
554 <https://doi.org/10.1016/j.envpol.2011.03.011>, 2011.
- 555 Cao, J., Yue, X. and Ma, M.: Simulation of ozone-vegetation coupling and feedback in

- 556 China using multiple ozone damage schemes, *Atmos. Chem. Phys.*, 24(7), 3973-  
557 3987, <https://doi.org/10.5194/acp-24-3973-2024>, 2024.
- 558 Chang, P., Zhang, S., Danabasoglu, G., Yeager, S.G., Fu, H., Wang, H., Castruccio, F.S.,  
559 Chen, Y., Edwards, J., Fu, D. and Jia, Y.: An unprecedented set of high-resolution  
560 earth system simulations for understanding multiscale interactions in climate  
561 variability and change, *J. Adv. Model. Earth. Sy.*, 12,  
562 <https://doi.org/10.1029/2020MS002298>, 2020.
- 563 Clifton, O. E., Paulot, F., Fiore, A. M., Horowitz, L. W., Correa, G., Baublitz, C. B.,  
564 Fares, S., Goded, I., Goldstein, A. H., Gruening, C., Hogg, A. J., Loubet, B.,  
565 Mammarella, I., Munger, J. W., Neil, L., Stella, P., Uddling, J., Vesala, T., and  
566 Weng, E.: Influence of Dynamic Ozone Dry Deposition on Ozone Pollution, *J.*  
567 *Geophys. Res-Atmos.*, 125, e2020JD032398,  
568 <https://doi.org/10.1029/2020JD032398>, 2020.
- 569 [Collatz, G. J., Ball, J. T., Grivet, C., and Berry, J. A.: Physiological and Environmental-](#)  
570 [Regulation of Stomatal Conductance, Photosynthesis and Transpiration – a Model](#)  
571 [That Includes a Laminar Boundary-Layer, \*Agr. Forest Meteorol.\*, 54, 107–136,](#)  
572 [doi:10.1016/0168-1923\(91\)90002-8, 1991.](#)
- 573 [Collatz, G. J., Ribas-Carbo, M., and Berry, J. A.: Coupled Photosynthesis-Stomatal](#)  
574 [Conductance Model for Leaves of C4 Plants, \*Aust. J. Plant Physiol.\*, 19, 519–538,](#)  
575 [https://doi.org/10.1071/PP9920519, 1992.](#)
- 576 Dizengremel, P.: Effects of ozone on the carbon metabolism of forest trees, *Plant.*  
577 *Physiol. Bioch.*, 39, 729–742, [https://doi.org/10.1016/S0981-9428\(01\)01291-8](https://doi.org/10.1016/S0981-9428(01)01291-8),  
578 2001.
- 579 Farquhar, G. D., von Caemmerer, S., and Berry, J. A.: A biochemical model of  
580 photosynthetic CO<sub>2</sub> assimilation in leaves of C<sub>3</sub> species, *Planta*, 149, 78–90,  
581 <https://doi.org/10.1007/BF00386231>, 1980.
- 582 [Feng, L., Smith, S. J., Braun, C., Crippa, M., Gidden, M. J., Hoesly, R., Klimont, Z.,](#)  
583 [van Marle, M., van den Berg, M., and van der Werf, G. R.: The generation of](#)  
584 [gridded emissions data for CMIP6, \*Geosci. Model Dev.\*, 13, 461–482,](#)  
585 [https://doi.org/10.5194/gmd-13-461-2020, 2020.](#)
- 586 Fiscus, E. L., Booker, F. L., and Burkey, K. O.: Crop responses to ozone: uptake, modes  
587 of action, carbon assimilation and partitioning, *Plant. Cell. Environ.*, 28, 997–1011,  
588 <https://doi.org/10.1111/j.1365-3040.2005.01349.x>, 2005.
- 589 Fuhrer, J., Skärby, L. and Ashmore, M.R.: Critical levels for ozone effects on vegetation  
590 in Europe, *Environ. Pollut.*, 97, 91-106, [https://doi.org/10.1016/S0269-](https://doi.org/10.1016/S0269-7491(97)00067-5)  
591 [7491\(97\)00067-5](https://doi.org/10.1016/S0269-7491(97)00067-5), 1997.
- 592 Gong, C., Lei, Y., Ma, Y., Yue, X., and Liao, H.: Ozone–vegetation feedback through

- 593 dry deposition and isoprene emissions in a global chemistry–carbon–climate  
594 model, *Atmos. Chem. Phys.*, 20, 3841–3857, [https://doi.org/10.5194/acp-20-](https://doi.org/10.5194/acp-20-3841-2020)  
595 3841-2020, 2020.
- 596 Gregg, J. W., Jones, C. G., and Dawson, T. E.: Physiological and Developmental Effects  
597 of O<sub>3</sub> on Cottonwood Growth in Urban and Rural Sites, *Ecol. Appl.*, 16, 2368–  
598 2381, [https://doi.org/10.1890/1051-0761\(2006\)016\[2368:PADEOO\]2.0.CO;2](https://doi.org/10.1890/1051-0761(2006)016[2368:PADEOO]2.0.CO;2),  
599 2006.
- 600 Hoesly, R. M., Smith, S. J., Feng, L., Klimont, Z., Janssens-Maenhout, G., Pitkanen, T.,  
601 Seibert, J. J., Vu, L., Andres, R. J., Bolt, R. M., Bond, T. C., Dawidowski, L.,  
602 Kholod, N., Kurokawa, J., Li, M., Liu, L., Lu, Z., Moura, M. C. P., O'Rourke, P.  
603 R., and Zhang, Q.: Historical (1750–2014) anthropogenic emissions of reactive  
604 gases and aerosols from the Community Emissions Data System (CEDS), *Geosci.*  
605 *Model. Dev.*, 11, 369–408, <https://doi.org/10.5194/gmd-11-369-2018>, 2018.
- 606 Huffman, G. J., Adler, R. F., Arkin, P., Chang, A., Ferraro, R., Gruber, A., Janowiak, J.,  
607 McNab, A., Rudolf, B., and Schneider, U.: The Global Precipitation Climatology  
608 Project (GPCP) Combined Precipitation Dataset, *B. Am. Meteorol. Soc.*, 78, 5–20,  
609 [https://doi.org/10.1175/1520-0477\(1997\)078<0005:TGPCPG>2.0.CO;2](https://doi.org/10.1175/1520-0477(1997)078<0005:TGPCPG>2.0.CO;2), 1997.
- 610 Hurtt, G. C., Chini, L., Sahajpal, R., Frolking, S., Bodirsky, B. L., Calvin, K., Doelman,  
611 J. C., Fisk, J., Fujimori, S., Klein Goldewijk, K., Hasegawa, T., Havlik, P.,  
612 Heinemann, A., Humpenöder, F., Jungclaus, J., Kaplan, J. O., Kennedy, J., Krisztin,  
613 T., Lawrence, D., Lawrence, P., Ma, L., Mertz, O., Pongratz, J., Popp, A., Poulter,  
614 B., Riahi, K., Shevliakova, E., Stehfest, E., Thornton, P., Tubiello, F. N., van  
615 Vuuren, D. P., and Zhang, X.: Harmonization of global land use change and  
616 management for the period 850–2100 (LUH2) for CMIP6, *Geosci. Model. Dev.*,  
617 13, 5425–5464, <https://doi.org/10.5194/gmd-13-5425-2020>, 2020.
- 618 Ito, G., Romanou, A., Kiang, N.Y., Faluvegi, G., Aleinov, I., Ruedy, R., Russell, G.,  
619 Lerner, P., Kelley, M. and Lo, K.: Global carbon cycle and climate feedbacks in  
620 the NASA GISS ModelE2, *J. Adv. Model. Earth. Sy.*, 12, [https://doi.org/](https://doi.org/10.1029/2019MS002030)  
621 10.1029/2019MS002030, 2020.
- 622 Jin, Z., Yan, D., Zhang, Z., Li, M., Wang, T., Huang, X., Xie, M., Li, S., and Zhuang,  
623 B.: Effects of Elevated Ozone Exposure on Regional Meteorology and Air Quality  
624 in China Through Ozone-Vegetation Coupling, *J. Geophys. Res-Atmos.*, 128,  
625 e2022JD038119, <https://doi.org/10.1029/2022JD038119>, 2023.
- 626 Jolivet, Y., Bagard, M., Cabané, M., Vaultier, M.-N., Gandin, A., Afif, D., Dizengremel,  
627 P., and Le Thiec, D.: Deciphering the ozone-induced changes in cellular processes:  
628 a prerequisite for ozone risk assessment at the tree and forest levels, *Ann. For. Sci.*,  
629 73, 923–943, <https://doi.org/10.1007/s13595-016-0580-3>, 2016.
- 630 Jung, M., Reichstein, M., ~~and Bondeau, A.: Towards global empirical upscaling of~~

- 631 ~~FLUXNET eddy covariance observations: validation of a model tree ensemble~~  
632 ~~approach using a biosphere model, Biogeosciences, 6, 2001–2013, 2009~~  
633 ~~Margolis, H.A., Cescatti, A., Richardson, A.D., Arain, M.A., Arneeth, A., Bernhofer, C.,~~  
634 ~~Bonal, D., Chen, J. and Gianelle, D.: Global patterns of land-atmosphere fluxes of~~  
635 ~~carbon dioxide, latent heat, and sensible heat derived from eddy covariance,~~  
636 ~~satellite, and meteorological observations. J. Geophys. Res-Biogeosci., 116(G3),~~  
637 ~~<https://doi.org/10.1029/2010JG001566>, 2011.~~
- 638 Kalnay, E., Kanamitsu, M., Kistler, R., Collins, W., Deaven, D., Gandin, L., Iredell, M.,  
639 Saha, S., White, G., Woollen, J., Zhu, Y., Chelliah, M., Ebisuzaki, W., Higgins, W.,  
640 Janowiak, J., Mo, K. C., Ropelewski, C., Wang, J., Leetmaa, A., Reynolds, R.,  
641 Jenne, R., and Joseph, D.: The NCEP/NCAR 40-Year Reanalysis Project, B. Am.  
642 Meteorol. Soc., 77, 437–472, [https://doi.org/10.1175/1520-0477\(1996\)077<0437:TNYRP>2.0.CO;2](https://doi.org/10.1175/1520-0477(1996)077<0437:TNYRP>2.0.CO;2), 1996.
- 644 Karlsson, P., Uddling, J., Braun, S., Broadmeadow, M., Elvira, S., Gimeno, B., Le Thiec,  
645 D., Oksanen, E., Vandermeiren, K., Wilkinson, M., and Emberson, L.: New critical  
646 levels for ozone effects on young trees based on AOT40 and simulated cumulative  
647 leaf uptake of ozone, Atmos. Environ., 38, 2283–2294,  
648 <https://doi.org/10.1016/j.atmosenv.2004.01.027>, 2004.
- 649 Koch, D., Schmidt, G. A., and Field, C. V.: Sulfur, sea salt, and radionuclide aerosols  
650 in GISS ModelE, J. Geophys. Res-Atmos, 111,  
651 <https://doi.org/10.1029/2004JD005550>, 2006.
- 652 [Laisk, A., Kull, O., & Moldau, H.: Ozone concentration in leaf intercellular air spaces](https://doi.org/10.1104/pp.90.3.1163)  
653 [is close to zero. Plant Physiol., 90\(3\), 1163-1167,](https://doi.org/10.1104/pp.90.3.1163)  
654 <https://doi.org/10.1104/pp.90.3.1163>, 1989.
- 655 Lam, J. C. Y., Tai, A. P. K., Ducker, J. A., and Holmes, C. D.: Development of an  
656 ecophysiology module in the GEOS-Chem chemical transport model version  
657 12.2.0 to represent biosphere–atmosphere fluxes relevant for ozone air quality,  
658 Geosci. Model. Dev., 16, 2323–2342, <https://doi.org/10.5194/gmd-16-2323-2023>,  
659 2023.
- 660 Lei, Y., Yue, X., Liao, H., Gong, C., and Zhang, L.: Implementation of Yale Interactive  
661 terrestrial Biosphere model v1.0 into GEOS-Chem v12.0.0: a tool for biosphere–  
662 chemistry interactions, Geosci. Model. Dev., 13, 1137–1153,  
663 <https://doi.org/10.5194/gmd-13-1137-2020>, 2020.
- 664 Lei, Y., Yue, X., Liao, H., Zhang, L., Yang, Y., Zhou, H., Tian, C., Gong, C., Ma, Y., and  
665 Gao, L.: Indirect contributions of global fires to surface ozone through ozone–  
666 vegetation feedback, Atmos. Chem. Phys., 21, 11531–11543,  
667 <https://doi.org/10.5194/acp-21-11531-2021>, 2021.
- 668 Li, Y., Henze, D.K., Jack, D.: The influence of air quality model resolution on health

- 669 impact assessment for fine particulate matter and its components, *Air. Qual. Atmos.*  
670 *Hlth.*, 9, 51-68, <https://doi.org/10.1007/s11869-015-0321-z>, 2016.
- 671 [Lin, M., Horowitz, L.W., Xie, Y., Paulot, F., Malyshev, S., Shevliakova, E., Finco, A.,](#)  
672 [Gerosa, G., Kubistin, D. and Pilegaard, K.: Vegetation feedbacks during drought](#)  
673 [exacerbate ozone air pollution extremes in Europe, \*Nat. Clim. Change.\*, 10,444-](#)  
674 [451, <https://doi.org/10.1038/s41558-020-0743-y>, 2020.](#)
- 675 Lombardozzi, D., Levis, S., Bonan, G., and Sparks, J. P.: Predicting photosynthesis and  
676 transpiration responses to ozone: decoupling modeled photosynthesis and stomatal  
677 conductance, *Biogeosciences*, 9, 3113–3130, [https://doi.org/10.5194/bg-9-3113-](https://doi.org/10.5194/bg-9-3113-2012)  
678 2012, 2012.
- 679 Lombardozzi, D., Sparks, J. P., and Bonan, G.: Integrating O<sub>3</sub> influences on terrestrial  
680 processes: photosynthetic and stomatal response data available for regional and  
681 global modeling, *Biogeosciences*, 10, 6815–6831, [https://doi.org/10.5194/bg-10-](https://doi.org/10.5194/bg-10-6815-2013)  
682 6815-2013, 2013.
- 683 Lombardozzi, D., Levis, S., Bonan, G., Hess, P. G., and Sparks, J. P.: The Influence of  
684 Chronic Ozone Exposure on Global Carbon and Water Cycles, *J. Climate.*, 28,  
685 292–305, <https://doi.org/10.1175/JCLI-D-14-00223.1>, 2015.
- 686 van Marle, M. J. E., Kloster, S., Magi, B. I., Marlon, J. R., Daniau, A.-L., Field, R. D.,  
687 Arneeth, A., Forrest, M., Hantson, S., Kehrwald, N. M., Knorr, W., Lasslop, G., Li,  
688 F., Mangeon, S., Yue, C., Kaiser, J. W., and van der Werf, G. R.: Historic global  
689 biomass burning emissions for CMIP6 (BB4CMIP) based on merging satellite  
690 observations with proxies and fire models (1750–2015), *Geosci. Model. Dev.*, 10,  
691 3329–3357, <https://doi.org/10.5194/gmd-10-3329-2017>, 2017.
- 692 Menon, S. and Rotstayn, L.: The radiative influence of aerosol effects on liquid-phase  
693 cumulus and stratiform clouds based on sensitivity studies with two climate  
694 models, *Clim. Dyn.*, 27, 345–356, <https://doi.org/10.1007/s00382-006-0139-3>,  
695 2006.
- 696 Mills, G., Buse, A., Gimeno, B., Bermejo, V., Holland, M., Emberson, L., and Pleijel,  
697 H.: A synthesis of AOT40-based response functions and critical levels of ozone  
698 for agricultural and horticultural crops, *Atmos. Environ.*, 41, 2630–2643,  
699 <https://doi.org/10.1016/j.atmosenv.2006.11.016> , 2007.
- 700 [Mills, G., Harmens, H., Wagg, S., Sharps, K., Hayes, F., Fowler, D., Sutton, M. and](#)  
701 [Davies, B.: Ozone impacts on vegetation in a nitrogen enriched and changing](#)  
702 [climate, \*Environ. Pollut.\*, 208, 898-908,](#)  
703 <https://doi.org/10.1016/j.envpol.2015.09.038>, 2016.
- 704 Myhre, G., Shindell, D., Breion, F.-M., Collins, W., Fuglestedt, J., Huang, J., Koch,  
705 D., Lamarque, J.-F., Lee, D., Mendoza, B., Nakajima, T., Robock, A., Stephens,

- 706 G., Takemura, T., and Zhang, H., Anthropogenic and Natural Radiative Forcing,  
707 in: *Climate Change 2013: The Physical Science Basis. Contribution of Working*  
708 *Group I to the Fifth Assessment Report of the Intergovernmental Panel on Climate*  
709 *Change*, edited by: Stocker, T. F., Qin, D., Plattner, G.-K., Tignor, M., Allen, S. K.,  
710 Boschung, J., Nauels, A., Xia, Y., Bex, V., and Midgley, P. M., Cambridge  
711 University Press, Cambridge, UK and New York, NY, USA, 2013.
- 712 Norval, M., Lucas, R. M., Cullen, A. P., De Gruijl, F. R., Longstreth, J., Takizawa, Y.,  
713 and Van Der Leun, J. C.: The human health effects of ozone depletion and  
714 interactions with climate change, *Photoch. Photobio. Sci.*, 10, 199–225,  
715 <https://doi.org/10.1039/C0PP90044C>, 2011.
- 716 Nussbaum, S. and Fuhrer, J.: Difference in ozone uptake in grassland species between  
717 open-top chambers and ambient air, *Environ. Pollut.*, 109, 463–471,  
718 [https://doi.org/10.1016/S0269-7491\(00\)00049-X](https://doi.org/10.1016/S0269-7491(00)00049-X), 2000.
- 719 Nuvolone, D., Petri, D., and Voller, F.: The effects of ozone on human health, *Environ.*  
720 *Sci. Pollut. R.*, 25, 8074–8088, <https://doi.org/10.1007/s11356-017-9239-3>, 2018.
- 721 Ohara, T., Akimoto, H., Kurokawa, J., Horii, N., Yamaji, K., Yan, X., and Hayasaka, T.:  
722 An Asian emission inventory of anthropogenic emission sources for the period  
723 1980–2020, *Atmos. Chem. Phys.*, 7, 4419–4444, [https://doi.org/10.5194/acp-7-](https://doi.org/10.5194/acp-7-4419-2007)  
724 [4419-2007](https://doi.org/10.5194/acp-7-4419-2007), 2007.
- 725 [Oleson, K. W., Lawrence, D. M., Bonan, G. B., Flanne, M. G., Kluzek, E., Lawrence,](#)  
726 [P. J., Levis, S., Swenson, S. C., and Thornton, P. E.: Technical Description of](#)  
727 [version 4.0 of the Community Land Model \(CLM\), National Center for](#)  
728 [Atmospheric Research, Boulder, USA, CONCAR/TN-478+STR, 2010.](#)
- 729 Oliver, R. J., Mercado, L. M., Sitch, S., Simpson, D., Medlyn, B. E., Lin, Y.-S., and  
730 Folberth, G. A.: Large but decreasing effect of ozone on the European carbon sink,  
731 *Biogeosciences*, 15, 4245–4269, 2018.
- 732 Petters, M. D. and Kreidenweis, S. M.: A single parameter representation of  
733 hygroscopic growth and cloud condensation nucleus activity, *Atmos. Chem. Phys.*,  
734 7, 1961–1971, <https://doi.org/10.5194/acp-7-1961-2007>, 2007.
- 735 [Paoletti, E., De Marco, A. and Rocalbuto, S.: Why should we calculate complex indices](#)  
736 [of ozone exposure? Results from Mediterranean background sites. \*Environ. Monit.\*](#)  
737 [Assess.](#), 128, pp.19-30, <https://doi.org/10.1007/s10661-006-9412-5>, 2007.
- 738 Pitchford, M., Malm, W., Schichtel, B., Kumar, N., Lowenthal, D., and Hand, J.:  
739 Revised Algorithm for Estimating Light Extinction from IMPROVE Particle  
740 Speciation Data, *Japca. J. Air. Waste. Ma.*, 57 (11), 1326–1336,  
741 <https://doi.org/10.3155/1047-3289.57.11.1326>, 2007.
- 742 Pleijel, H., Danielsson, H., Ojanperä, K., Temmerman, L. D., Högy, P., Badiani, M.,

- 743 and Karlsson, P. E.: Relationships between ozone exposure and yield loss in  
744 European wheat and potato—a comparison of concentration- and flux-based  
745 exposure indices, *Atmos. Environ.*, 38, 2259–2269,  
746 <https://doi.org/10.1016/j.atmosenv.2003.09.076>, 2004.
- 747 Pleijel, H., Danielsson, H., Emberson, L., Ashmore, M. R., and Mills, G.: Ozone risk  
748 assessment for agricultural crops in Europe: further development of stomatal flux  
749 and flux–response relationships for European wheat and potato, *Atmos. Environ.*,  
750 41, 3022–3040, <https://doi.org/10.1016/j.atmosenv.2006.12.002>, 2007.
- 751 Remer, L. A., Kaufman, Y. J., Tanré, D., Mattoo, S., Chu, D. A., Martins, J. V., Li, R.-  
752 R., Ichoku, C., Levy, R. C., and Kleidman, R. G.: The MODIS aerosol algorithm,  
753 products, and validation, *J. Atmos. Sci.*, 62, 947–973,  
754 <https://doi.org/10.1175/JAS3385.1>, 2005.
- 755 Sadiq, M., Tai, A. P., Lombardozzi, D., and Val Martin, M.: Effects of ozone–vegetation  
756 coupling on surface ozone air quality via biogeochemical and meteorological  
757 feedbacks, *Atmos. Chem. Phys.*, 17, 3055–3066, [https://doi.org/10.5194/acp-17-](https://doi.org/10.5194/acp-17-3055-2017)  
758 [3055-2017](https://doi.org/10.5194/acp-17-3055-2017), 2017.
- 759 Schmidt, G. A., Ruedy, R., Hansen, J. E., Aleinov, I., Bell, N., Bauer, M., Bauer, S.,  
760 Cairns, B., Canuto, V., Cheng, Y., Genio, A. D., Faluvegi, G., Friend, A. D., Hall,  
761 T. M., Hu, Y., Kelley, M., Kiang, N. Y., Koch, D., Lacis, A. A., Lerner, J., Lo, K.  
762 K., Miller, R. L., Nazarenko, L., Oinas, V., Perlwitz, J., Perlwitz, J., Rind, D.,  
763 Romanou, A., Russell, G. L., Sato, M., Shindell, D. T., Stone, P. H., Sun, S.,  
764 Tausnev, N., Thresher, D., and Yao, M.-S.: Present-Day Atmospheric Simulations  
765 Using GISS ModelE: Comparison to In Situ, Satellite, and Reanalysis Data, *J.*  
766 *Climate.*, 19, 153–192, <https://doi.org/10.1175/JCLI3612.1>, 2006.
- 767 Schmidt, G. A., Kelley, M., Nazarenko, L., Ruedy, R., Russell, G. L., Aleinov, I., Bauer,  
768 M., Bauer, S. E., Bhat, M. K., Bleck, R., Canuto, V., Chen, Y.-H., Cheng, Y., Clune,  
769 T. L., Del Genio, A., de Fainchtein, R., Faluvegi, G., Hansen, J. E., Healy, R. J.,  
770 Kiang, N. Y., Koch, D., Lacis, A. A., LeGrande, A. N., Lerner, J., Lo, K. K.,  
771 Matthews, E. E., Menon, S., Miller, R. L., Oinas, V., Olosó, A. O., Perlwitz, J. P.,  
772 Puma, M. J., Putman, W. M., Rind, D., Romanou, A., Sato, M., Shindell, D. T.,  
773 Sun, S., Syed, R. A., Tausnev, N., Tsigaridis, K., Unger, N., Voulgarakis, A., Yao,  
774 M.-S., and Zhang, J.: Configuration and assessment of the GISS ModelE2  
775 contributions to the CMIP5 archive: GISS MODEL-E2 CMIP5 SIMULATIONS,  
776 *J. Adv. Model. Earth Syst.*, 6, 141–184, <https://doi.org/10.1002/2013MS000265>,  
777 2014.
- 778 [Sicard, P., De Marco, A., Dalstein-Richier, L., Tagliaferro, F., Renou, C., Paoletti, Elena,](#)  
779 [2016. An epidemiological assessment of stomatal ozone flux-based critical levels](#)  
780 [for visible ozone injury in southern European forests. \*Sci. Total. Environ.\*, 541,](#)  
781 [729-741.](#)

- 782 Sitch, S., Cox, P. M., Collins, W. J., and Huntingford, C.: Indirect radiative forcing of  
783 climate change through ozone effects on the land-carbon sink, *Nature*, 448, 791–  
784 794, <https://doi.org/10.1038/nature06059>, 2007.
- 785 [Sofen, E. D., Bowdalo, D., Evans, M. J., Apadula, F., Bonasoni, P., Cupeiro, M., Ellul,](#)  
786 [R., Galbally, I. E., Girgzdiene, R., Luppo, S., Mimouni, M., Nahas, A. C., Saliba,](#)  
787 [M., and Tørseth, K.: Gridded global surface ozone metrics for atmospheric](#)  
788 [chemistry model evaluation, \*Earth Syst. Sci. Data\*, 8, 41–59,](#)  
789 <https://doi.org/10.5194/essd-8-41-2016>, 2016.
- 790 Unger, N., Zheng, Y., Yue, X., and Harper, K. L.: Mitigation of ozone damage to the  
791 world’s land ecosystems by source sector, *Nat. Clim. Chang.*, 10, 134–137,  
792 <https://doi.org/10.1038/s41558-019-0678-3>, 2020.
- 793 VanLoocke, A., Betzelberger, A. M., Ainsworth, E. A., and Bernacchi, C. J.: Rising  
794 ozone concentrations decrease soybean evapotranspiration and water use  
795 efficiency whilst increasing canopy temperature, *New. Phytol.*, 195, 164–171,  
796 <https://doi.org/10.1111/j.1469-8137.2012.04152.x>, 2012.
- 797 van der Werf, G. R., Randerson, J. T., Giglio, L., van Leeuwen, T. T., Chen, Y., Rogers,  
798 B. M., Mu, M., van Marle, M. J. E., Morton, D. C., Collatz, G. J., Yokelson, R. J.,  
799 and Kasibhatla, P. S.: Global fire emissions estimates during 1997–2016, *Earth*  
800 *Syst. Sci. Data*, 9, 697–720, <https://doi.org/10.5194/essd-9-697-2017>, 2017.
- 801 Wang, Y., Shen, L., Wu, S., Mickley, L., He, J. and Hao, J.: Sensitivity of surface ozone  
802 over China to 2000–2050 global changes of climate and emissions, *Atmos.*  
803 *Environ*, 75, 374–382, <https://doi.org/10.1016/j.atmosenv.2013.04.045>, 2013.
- 804 Wesely, M. L. and Hicks, B. B.: A review of the current status of knowledge on dry  
805 deposition, *Atmos. Environ.*, 34, 2261–2282, [https://doi.org/10.1016/S1352-](https://doi.org/10.1016/S1352-2310(99)00467-7)  
806 [2310\(99\)00467-7](https://doi.org/10.1016/S1352-2310(99)00467-7), 2000.
- 807 Wild, M., Folini, D., Schär, C., Loeb, N., Dutton, E. G., and König-Langlo, G.: The  
808 global energy balance from a surface perspective, *Clim. Dyn.*, 40, 3107–3134,  
809 <https://doi.org/10.1007/s00382-012-1569-8>, 2013.
- 810 Yue, X., Liao, H., Wang, H. J., Li, S. L., and Tang, J. P.: Role of sea surface temperature  
811 responses in simulation of the climatic effect of mineral dust aerosol, *Atmos.*  
812 *Chem. Phys.*, 11, 6049–6062, <https://doi.org/10.5194/acp-11-6049-2011>, 2011.
- 813 Yue, X. and Unger, N.: Ozone vegetation damage effects on gross primary productivity  
814 in the United States, *Atmos. Chem. Phys.*, 14, 9137–9153,  
815 <https://doi.org/10.5194/acp-14-9137-2014>, 2014.
- 816 Yue, X. and Unger, N.: The Yale Interactive terrestrial Biosphere model version 1.0:  
817 description, evaluation and implementation into NASA GISS ModelE2, *Geosci.*  
818 *Model Dev.*, 8, 2399–2417, <https://doi.org/10.5194/gmd-8-2399-2015>, 2015.

- 819 Yue, X. and Unger, N.: Fire air pollution reduces global terrestrial productivity, *Nat.*  
820 *Commun.*, 9, 5413, <https://doi.org/10.1038/s41467-018-07921-4>, 2018.
- 821 Yue, X., Keenan, T. F., Munger, W., and Unger, N.: Limited effect of ozone reductions  
822 on the 20-year photosynthesis trend at Harvard forest, *Glob. Change Biol.*, 22,  
823 3750–3759, <https://doi.org/10.1111/gcb.13300>, 2016.
- 824 Yue, X., Liao, H., Wang, H., Zhang, T., Unger, N., Sitch, S., Feng, Z., and Yang, J.:  
825 Pathway dependence of ecosystem responses in China to 1.5°C global warming,  
826 *Atmos. Chem. Phys.*, 20, 2353–2366, <https://doi.org/10.5194/acp-20-2353-2020>,  
827 2020.
- 828 Zhang, L., Vet, R., Brook, J. R., and Legge, A. H.: Factors affecting stomatal uptake of  
829 ozone by different canopies and a comparison between dose and exposure, *Sci.*  
830 *Total Environ.*, 370, 117–132, <https://doi.org/10.1016/j.scitotenv.2006.06.004>,  
831 2006.
- 832 Zhou, X., Yue, X., and Tian, C.: Responses of Ecosystem Productivity to Anthropogenic  
833 Ozone and Aerosols at the 2060, *Earths Future*, 12, e2023EF003781,  
834 <https://doi.org/10.1029/2023EF003781>, 2024.
- 835 Zhu, J., Tai, A. P. K., and Hung Lam Yim, S.: Effects of ozone–vegetation interactions  
836 on meteorology and air quality in China using a two-way coupled land–  
837 atmosphere model, *Atmos. Chem. Phys.*, 22, 765–782,  
838 <https://doi.org/10.5194/acp-22-765-2022>, 2022.
- 839